Habitable Planet, 2026, 2(2), 391–412

Scilight

Habitable Planet

Journal Homepage: https://www.sciltp.com/journals/hp

Check for updates

Review

Orogenic Gold Mineralization in the Dharwar Craton: Current Understanding and the Enigma of Auriferous Fluid Sources

Sakthi Saravanan Chinnasamy[1,*], Manash Jyoti Saikia[1,#], Debasis Pal[2], and Manju Sati[3,$]

[1] Department of Earth Sciences, Indian Institute of Technology Bombay, Powai, Mumbai 400076, India
[2] Department of Applied Science and Humanities, Purnea College of Engineering, Bihar Engineering University (Patna), DSTTE, Patna, Purnea 854303, India
[3] Department of Earth Sciences, Indian Institute of Technology, Roorkee 247667, India
[*] Correspondence: chinnasamys@iitb.ac.in. Present Addresses: # Regional Office, Indian Bureau of Mines, Guwahati 781006, India; $ Department of Earth Sciences, University of New Brunswick (UNB), Canada.

ABSTRACT

The Dharwar Craton of southern India hosts one of the most significant Neoarchean gold provinces in the world and contains numerous economically important gold deposits distributed across the Eastern and Western Dharwar Cratons. This review synthesizes geological, structural, metamorphic, geochronological, fluid inclusion, stable isotope, and accessory mineral geochemical data to develop a comprehensive understanding of the genesis of these gold systems and their implications for mineral exploration. Gold mineralization is predominantly localized within brittle–ductile shear zones, higher-order structural splays, and lithological contacts, highlighting the critical role of transcrustal deformation in focusing hydrothermal fluids. Hydrothermal alteration is characterized by pervasive carbonatization, sericitization, chloritization, silicification, sulfidation, and locally tourmalinization, forming consistent alteration halos around mineralized zones. Available geochronological constraints indicate that the principal mineralization event occurred between ca. 2547 and 2510 Ma, broadly synchronous with regional metamorphism, juvenile granitoid magmatism, and late Neoarchean tectonic reworking. Fluid inclusion studies reveal predominantly low- to moderately saline H_2O–CO_2–NaCl $\pm$ CH_4 fluids formed under mesothermal conditions, whereas stable isotope compositions (O–H–C–S and Sr) indicate a dominant metamorphic signature with localized magmatic/ juvenile contributions. Gold deposition was primarily facilitated by pressure fluctuations, fluid immiscibility, sulfidation of reactive host rocks, and fluid–rock interaction within active shear systems. Geochemical signatures preserved in accessory minerals, particularly tourmaline, pyrite, and arsenopyrite, further document episodic fluid flow and evolving hydrothermal conditions during ore formation. The temporal overlap between bimodal volcanism, greenstone metamorphism, juvenile granitoid emplacement, and gold mineralization, together with the remarkable consistency of ore-fluid compositions and isotopic signatures across the craton, supports a mixed fluid-source model in which metamorphic devolatilization supplied the dominant ore fluids while juvenile magmatism contributed heat and locally volatile-rich components. This integrated synthesis reinforces the classification of Dharwar gold deposits as classic Archean orogenic systems and provides a robust mineral systems framework for future exploration targeting and genetic investigations. The combined approach of host/altered rock minerology, geochemistry, and fluid inclusion and stable/radiogenic isotopic studies are useful to propose a holistic model for formation of orogenic gold mineralization in Dharwar Craton and beyond.

ARTICLE INFO

History:

Received: 28 April 2026
Revised: 18 May 2026
Accepted: 30 June 2026
Published: 08 July 2026

Keywords:

Dharwar Craton; greenstone belts; orogenic gold; fluid source

Citation:

Chinnasamy, S.S.; Saikia, M.J.; Pal, D.; et al. Orogenic Gold Mineralization in the Dharwar Craton: Current Understanding and the Enigma of Auriferous Fluid Sources. *Habitable Planet* **2026**, *2*(2), 391–412. https://doi.org/10.63335/j.hp.2026.0045

Copyright: © 2026 by the authors. This is an open access article under the terms and conditions of the Creative Commons Attribution (CC BY) license (https://creativecommons.org/licenses/by/4.0/).
Publisher's Note: Scilight stays neutral with regard to jurisdictional claims in published maps and institutional affiliations.

Research Highlights

- Genesis of gold systems in the Archean Dharwar Craton.
- Mixed fluid-source model in which metamorphic devolatilization supplied the dominant ore fluids.
- Juvenile magmatism contributed heat and locally volatile-rich components.
- A holistic model for formation of orogenic gold mineralization in Dharwar Craton and beyond.

1. Introduction

Orogenic gold deposits comprise approximately 75% of worldwide gold resources and are the predominant genetic class of gold deposits generated inside structurally controlled, crustal-scale hydrothermal processes [1]. Archean orogenic lode-gold deposits, in particular, are widely developed within regionally metamorphosed granite–greenstone terranes and account for approximately 30% of the world's gold production [2]. These include some of the world's most significant deposits and camps, such as the Golden Mile of the Yilgarn Craton (Western Australia), the Hollinger–McIntyre and Timmins deposits of the Abitibi belt (Canada), and the giant Kolar deposit of the Dharwar Craton (southern India). Furthermore, there are many more Archean cratons that have rich orogenic gold provinces. These include the Superior and Slave Cratons in Canada, Tanzania Craton, Kaapvaal Craton in southern Africa, Zimbabwe Craton, São Francisco Craton in South America, and the Dharwar Craton in India. Despite their global abundance, the genesis of orogenic gold deposits remains contentious due to their occurrence across a broad spectrum of pressure–temperature conditions, diverse host lithologies, and wide crustal levels, coupled with the inherent inaccessibility of active mineralizing systems. The term "orogenic gold" was first coined by [3] and later formalized by [4], who's widely used "crustal continuum model" proposed that these deposits form along trans crustal fault systems under metamorphic conditions ranging from sub-greenschist to amphibolite facies [5]. Although significant, this model has been modified in later studies to address uncertainty about fluid sources, metal solubility, and physicochemical limits on gold transport and deposition [6–9]. The nature and source of ore fluids, the ligands involved in gold complexation and transportation, the function of crustal-scale structures as fluid conduits, and the mechanism of gold precipitation, including fluid–rock interaction, phase separation, and fluid mixing, are common genetic questions [8–10]. Among them the source of fluid remains an important question even after three decades of research on orogenic gold deposits worldwide.

In India, Dharwar Craton, has been divided into two blocks such as Western (WDC), and Eastern (EDC) separated by significant shear zones (Figure 1; [11]). Each block has a distinct magmatic and geological evolution that affects the gold mineralization. In the two blocks, WDC is characterized by sedimentary dominant along with subordinate volcanic greenstone sequences globally linked TTG gneisses and potassic plutons. EDC contains linear greenstone belts with subordinate sediments, transitional TTGs, diatexites, and calc-alkaline plutons [11]. The two contrasting geological domains host several major well known gold camps i.e., Kolar, Hutti, Uti, Hira-Buddini, Ramagiri–Penakacherla and Sandur in the EDC; and Gadag, Ajjanahalli, G.R. Halli, and Paramanahalli in the WDC. Fluid inclusion studies over the craton wide deposits show low-salinity aqueous-carbonic fluids, $H_2O + CO_2 \pm N_2 \pm NaCl \pm CH_4$ with exceptions such as Uti CO_2-poor mineralizing fluids [12]. Despite significant geological and geochronological studies, the links between magmatism, greenstone metamorphism, and gold mineralization remain equivocal, and the origin of auriferous fluids is still subject to debate as similar to the orogenic gold deposits elsewhere. This review presents a synthesis of the Dharwar Craton's geological framework and evaluates the genetic characteristics of key gold camps within the cratons and its greenstone belts, in light of recent insights into Archean orogenic processes and gold mineralization. The combined approach of filed geology, structures, mineralogy, greenstone metamorphism, hydrothermal alterations, geochemistry of mineralized zones, geochronology, fluid inclusion studies, and stable isotopic signature used to provide a comprehensive holistic model, which can be helpful to target mineralizing area, in similar setting in the Dharwar Craton and beyond.

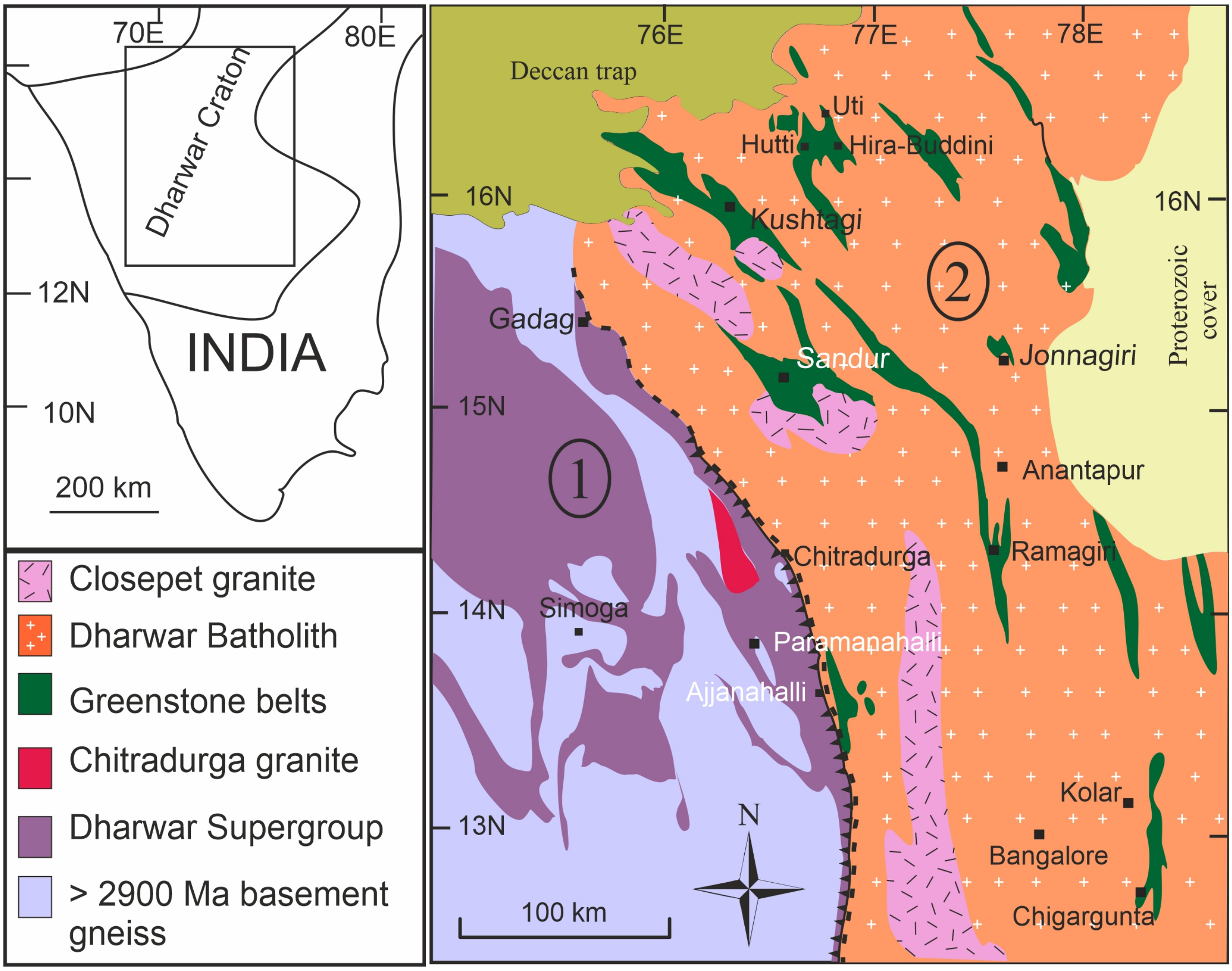

Figure 1. Regional geological map of the Dharwar craton in southern India showing major gold hosting greenstone belts in three distinct crustal blocks (1) Western Dharwar craton, WDC (2) Eastern Dharwar craton, EDC (modified after [11]).

2. Geology and Mineralization Characteristic of Orogenic Gold Deposits in the Dharwar Craton

2.1. Hutti-Maski Greenstone Belt (HMGB)

The hook-shaped Hutti-Maski Greenstone Belt (HMGB) of the EDC is made up of predominantly mafic and felsic volcanic rocks with subordinate sedimentary layers that lie unconformably on the Peninsular Gneissic Complex (PGC) [13, 14]. The belt extends approximately 45 km east-west and 80 km north-south, and it is surrounded by significant sinistral shear zones [15]. HMGB is known to host world-class Hutti, Uti, and Hira-Buddini gold deposits. According to [16, 17], gold mineralization at Hutti is epigenetic, structurally controlled, and mostly contained within metavolcanic rocks that are composed of felsic volcanic layers interlayered with fine-grained to massive and pillowed tholeiitic amphibolites. Three metamorphic stages (M_1–M_3) and five deformation phases (D_1–D_5) are identified by structural studies [13, 18]. D_2/M_2 and D_3/M_3 correspond to two significant mineralizing events. Fine native gold can be found along pyrite grain boundaries or as inclusions inside pyrite and arsenopyrite in stage-1 mineralization. According to [15], laminated quartz veins containing scheelite, pyrrhotite, chalcopyrite, arsenopyrite, and pyrite host stage-2 mineralization that locally reaches values of up to 1 kg/t Au. Amphibolites and felsic volcanics predominate in the Uti deposit, which is situated in the northern HMGB, with a small amount of quartz-mica schist. Three stages of folding over the belt are documented by regional structural investigations [19, 20]. Similar oriented D_2 foliations overprint steeply dipping ($\geq 80°$) D_1 shear foliations at Uti. Broad open F_3 folds with axial planes that trend NE–SW are indicative of a third deformation phase (D_3) [12]. Seventeen auriferous lodes, each with strike lengths of 50–700 m and thicknesses of 0.3–24 m, have been identified by the Geological Survey of India (GSI) and Hutti Gold Mines Ltd. (HGML) together. An estimated reserve of 6.51 Mt to a depth of 60 m with an average grade of 2.64 g/t Au is found in Lode-4 alone [21]. Gold occurs primarily in metabasites along shear zones that trend NNE–SSW. The hydrothermal mineral assemblage includes biotite, K-feldspar, actinolite, and titanite. According to [12], pyrrhotite and arsenopyrite are locally found with invisible gold. The Hira-Buddini deposit, which is situated 19 km east of Hutti, contains gold mineralization in a brittle-ductile shear zone at contact of amphibolite and metamorphosed felsic volcanics. According to [22], drilling revealed about 200 kt of high-grade ore (6–10 g/t Au) down to a of 145 m. Fault-filled quartz veins that are accompanied by sub-horizontal sigmoidal extensional veins undergo mineralization [23]. According to [24], pore-fluid pressures above the minimal main stress plus tensile strength promote hydraulic fracturing during vein formation, thereby explain the sub-horizontal sigmoidal veins formation in contrast to those formed at Hutti.

2.2. Kolar Greenstone Belt (KGB)

One of the world's renowned and classic Archean orogenic gold provinces is the Kolar Gold Field (KGF), which is located in the core of Kolar greenstone belt in EDC. According to [25], the field is around 81 km long and 3–4 km wide. The older Kambha granodiorite gneiss to the east and the newer Dod and Dosa granite gneisses to the west provide the structural boundaries of the amphibolite-facies metavolcanics, which host the majority of the mineralization. At KGF, ore shoots were oriented along foliation-parallel shear zones, and gold-bearing lodes were deposited throughout several stages of ductile deformation [26, 27]. According to [28–30], KGF historically produced about 794 tons of gold by 1987, with remarkably high grades (up to ∼25 g/t) reported from the Champion lode. In 2001, the mine was shut down because to declining ore grades (∼2–3 g/t). In contrast to the McTaggart and Oriental lodes, which are sulfide-rich and include occurrence of gold inclusions in arsenopyrite and pyrrhotite within the Nundydroog mine. The Champion lode has sulfide-poor, quartz–calcite veins that contain free native gold. A number of historically significant deposits, such as Chigargunta (CG) and Bisanatham (BN), as well as new prospects, including Mallappakonda, Yerakonda, Virupakshipura–Lakkhanayakhanhalli (New BN), Kudithanapalli, Sanganapalli, and Peddapartikunta, are well known to host gold mineralization which are located in south of the main KGF district called South Kolar Greenstone Belt (SKGB) [31, 32].

2.3. South Kolar Greenstone Belt (SKGB)

The SKGB, the southern extension of the Kolar Schist Belt, covers approximately 50 km^2 and extends for nearly 30 km in a north–south direction with a maximum width of about 3 km. In the SKGB, gold deposition is concentrated in structurally controlled sheared quartz-carbonate veins. Ore localization is first-order controlled by tight isoclinal folds with north-south trending, steeply dipping axial planes (67°–88°) and a regionally continuous, shear-parallel foliation that stretches over 30 km and dips sharply both eastward and westward [29, 30]. Ongoing exploration by private entities and the National Mineral Development Corporation's (NMDC) recent acquisition of CG and BN gold blocks demonstrate the gold district's increased strategic significance [31].

The belt is dominated by Champion gneiss and metabasalts, with subordinate carbonaceous phyllite, greywacke, and BIF. Gold mineralization extends from Bisanatham (BN) in the north to Maharajagadai in Tamil Nadu through Chigargunta (CG), encompassing several historical mines and prospects, including CG, BN, Mallappakonda, Yerakonda, Virupakshipura–Lakkhanayakhanhalli (New BN), Kudithanapalli, Sanganapalli, and Peddapartikunta. Mineralization is largely concentrated near the contact between Champion gneiss and metabasalts and is characterized by intense sulfidation dominated by pyrite and pyrrhotite, except at Kudithanapalli where molybdenite is abundant. The belt experienced lower amphibolite-facies metamorphism (∼4.6 kbar and ∼600 °C) at 2546 ± 12 Ma, followed by retrograde decompression and hydrothermal overprinting [32, 33].

The Chigargunta deposit is located near the Andhra Pradesh–Karnataka–Tamil Nadu border and is one of the most important gold occurrences in the SKGB. Mafic greenstones comprising metabasalts and metagabbros dominate the western part of the area, whereas the central and eastern portions are occupied by Champion gneiss, composed mainly of felsic volcanic rocks with characteristic quartz blebs. Gold mineralization is localized within brittle–ductile shear zones and sheared quartz–carbonate veins hosted predominantly by Champion gneiss (Figure 2a), although some lodes occur along contacts with metabasalts. Ore localization is controlled by north–south-trending, steeply dipping shear-parallel foliations and tight isoclinal folds with axial planes dipping between 67° and 88° [32]. Two principal vein systems extend for nearly 3 km with widths ranging from 0.5 to 2.5 m and continue to depths exceeding 300 m. The deposit contains an estimated resource of approximately 12 tonnes of gold at an average grade of 5.66 g/t and remains a focus of ongoing exploration.

The Bisanatham deposit comprises two distinct mineralized systems: the eastern Old BN mine and the western New BN prospect. The Old BN mine is hosted within schistose metabasalts and amphibolites adjacent to Champion gneiss and is structurally associated with an antiformal fold cored by the Bisanatham granite. Gold occurs in north–south-striking quartz veins dipping 60–80° west and is distributed in three principal lodes exhibiting en-echelon ore shoots extending to depths of about 300 m. Reported gold grades range from 1.12 to 7.13 g/t, with historical production of approximately 300 kg of gold at an average grade of 3.5 g/t.

The New BN prospect is hosted within pillowed metabasalts and comprises eastern and central lode systems extending over at least 400 m. Mineralization is associated with localized shear zones and quartz veins enriched in sulfides, accompanied by intense hydrothermal alteration including biotite and carbonate development. The eastern lode follows the contact between schistose metabasalts and felsic volcanic rocks and exhibits a steep westward dip. Geological, structural, and alteration characteristics closely resemble those of the Champion lodes of the Kolar Gold Field, emphasizing the importance of shear-controlled hydrothermal fluid flow and lithological contacts in localizing gold mineralization throughout the SKGB.

2.4. Jonnagiri Greenstone Belt (JGB)

Jonnagiri greenstone belt is composed of Neoarchean volcano–sedimentary sequence dominated by mafic to felsic metavolcanics, volcanic tuffs, and syn-volcanic gabbroic to ultramafic sills, located in EDC. Two separate granitoid magmatic pulses, represented by the younger Chennampalli granite and the older Pagadarayi granodiorite, crosscut the supracrustal package after several gabbroic and doleritic dikes [34–36]. According to structural analysis, the greenstone belt underwent two major folding events (F_1 and F_2), both of which are linked to the axial-planar foliations S_1 and S_2. According to [34], shearing that occurred along with F_2 deformation provided the belt a prominent sigmoidal shape. Two generations of shear foliations (Sh_1, Sh_2) and well-developed *S–C* fabrics, suggesting both dextral and sinistral shear direction, are indicative of deformation history of intrusive Pagadarayi granodiorite [35, 36] where majority of gold mineralization is occurring in the Sh_2 N–S oriented quartz veins (Figure 2b). Jonnagiri gold deposit is famous for granitoid-hosted mineralization, linked to the Pagadarayi granodiorite. At a cut-off grade of 1.0 g/t, the deposit has a likely resource of about 15 tons of gold to depths $\leq$180 m [37]. Ore is generally found in fracture-filled quartz veins and auriferous pyrite, where gold is found in sulfide assemblages of the inner mineralized zone as micro- to nanoscale particles as well as tiny inclusions. A reduced, sulfur-rich ore fluid characteristic of many Archean orogenic systems is further reflected by the presence of gold in fracture filling within thin quartz veins and close proximity to FeS_2–$Fe_{2-x}S$ (pyrite–pyrrhotite) assemblages, buffered near the fs_2 stability field.

2.5. Ramagiri Greenstone Belt (RGB)

Ramagiri–Penakacherla greenstone belt, lies on the western side of the EDC, made up of several granitoids, that have intruded into volcanic-dominated supracrustal rocks. In the early 20th century, the deposit was a major producer of gold, producing about 5 tons of gold at an average grade of about 15 g/t [38]. The host rocks are dark to light grey phyllites, in which the auriferous veins are mostly found. The mineralized vein has an assemblage of quartz $\pm$ carbonate $\pm$ sulfide, and emplaced along significant brittle–ductile shear zones are the predominant hosts of gold mineralization. Pyrite and chalcopyrite are major sulfide minerals found with gold in the mineralized zones [39]. The deformation played an important role in localizing mineralizing fluids in this region of the EDC and lead to responsible for gold deposition.

2.6. Chitradurga Greenstone Belt (CGB)

Gadag, Ajjanahalli, G.R. Halli, and Paramanahalli are notable gold deposits and prospects located in CGB in WDC. Gadag Gold Field (GGF) is located in the Gadag Greenstone Belt (GGB) in the northern part of the CGB. According to [40], mineralization occurred in three different litho-domains: (1) metavolcanics in the western auriferous zone (average grade: 4.02 g/t); (2) a turbidite sequence in the central zone (average grade: 4.77 g/t); and (3) BIF interlayered with phyllite in the eastern zone (average grade: $\sim$2 g/t). represented as three auriferous lodes western, central, and Eastern lodes respectively. Second-order splays connected to the main shear structures that make up the “Gadag Duplex” regulate the spatial distribution of gold mineralization in the GGF [41]. Gold can be found in quartz, silicates, and sulfides, especially arsenopyrite. Gold can occur as the form of tiny blebs, irregular patches, and thin stringers in both quartz lodes and altered wall rocks.

The GGB covers an area of approximately 2400 km^2 south of Gadag town and constitutes one of the most important Archean gold-bearing terranes in southern India. It is widely regarded as the northern continuation of the Chitradurga Greenstone Belt and is thought to have formed during the accretion of the Eastern and Western Dharwar Cratons between ca. 2.7 and 2.51 Ga. The belt, also referred to as the “Gadag Duplex,” represents a tectonic assemblage produced by large-scale thrust stacking and imbrication of volcano-sedimentary sequences during Neoarchean crustal convergence. It comprises metavolcanic rocks ranging from basaltic to rhyolitic and andesitic compositions, together with metasedimentary units including greywacke, polymictic conglomerate, ferruginous chert, carbonaceous phyllite, and banded iron formation (BIF), all enclosed by tonalite–trondhjemite–granodiorite (TTG) gneisses and younger K-rich granites. Well-preserved primary features such as pillow structures in metavolcanics and cross-bedding, graded bedding, and convolute laminations in sedimentary rocks indicate excellent preservation of the original depositional environment [42].

The regional architecture of the GGB is dominated by N–S to NW–SE structural trends developed during E–W compression and uplift. A major mylonitic thrust zone along the eastern margin, corresponding to the Chitradurga Thrust, marks the tectonic boundary between Archean supracrustal rocks and younger granitoids. Orogenic gold mineralization occurs as a series of linear lodes hosted by metabasalts, BIF, and metasedimentary rocks, with individual lodes extending between 2 and 12 km. The close spatial association between quartz–carbonate veins, shear zones, and the Gadag Duplex demonstrates that gold deposition was strongly controlled by regional deformation and fluid flow along structurally prepared pathways.

Structurally, the GGB records three principal deformation events. The earliest deformation (D_1) generated NW–SE-trending, tight to isoclinal folds and penetrative fabrics, whereas the second deformation (D_2) produced

NNW–SSE-trending shear zones and upright to tight folds that define the present geometry of the belt. A weaker third deformation (D_3), characterized by E–W axial traces and interpreted to result from NE–SW compression, overprinted the earlier structures and contributed to the development of dome-and-basin patterns. The recognition of deep-rooted NE–SW faults/shears cutting earlier fabrics further highlights the complex tectonic evolution of the belt (Figure 2c). Together, the multistage deformation, amphibolite-grade metamorphism, and long-lived shear systems provided favourable conditions for focusing hydrothermal fluids and localizing economically significant Archean orogenic gold mineralization in the Gadag Greenstone Belt [42].

Ajjanahalli gold deposit is an epigenetic, structurally controlled and hosted within BIF. The BIF sequence has undergone three phases of folding from early tight to isoclinal F_1 folds to late F_3 upright folds [43]. Gold mineralization is primarily associated with shearing synchronous with F_2 folding, developed under a relatively low-stress regime compared with the high-strain Chitradurga shear zone located a few km to the east. Mineralization is concentrated in the nose region of a large, north-plunging anticline, where F_2 axial-plane–parallel quartz veins and the sigmoidal, fracture-filled gash veins within the BIF served as effective fluid pathways. During fluid–rock interaction, primary oxides were replaced by sulfides, and gold was subsequently sequestered as inclusions within pyrite and along pyrite-pyrrhotite grain contacts [44].

Paramanahalli gold deposit situated in the south-central region of the CGB discovered by GSI in 2004 [45]. Gold mineralization is associated with altered metabasalt and banded iron formation (BIF) of the Hiriyur Formation, Dharwar Supergroup. The NNW–SSE trending Chitradurga Shear Zone, which served as the main channel for hydrothermal fluid movement, structurally controls gold mineralization [46, 47]. Major changes that occurred during fluid–rock interaction and the subsequent deposition of sulfides and gold such as carbonatization, chloritization, silicification, and sulfidation. The deposit preserves indications of both brittle and ductile deformation, such as folding, shearing (Figure 2d), faulting, brecciation, and joints all of which increased permeability and promoted focused fluid flow. In carbonated metabasalts, BIF, and quartz-ankerite veins, mineralization takes the form of dispersed sulfides. The three main sulfides linked to gold are pyrite, chalcopyrite, and pyrrhotite. Fe-rich hydrothermal chlorite is found in the proximal alteration zone and is strongly linked to gold-bearing sulfide assemblages. Hence, the chlorite thermometry shows temperatures between 306 and 326 °C, which are compatible with the mesothermal type of Archean orogenic gold deposits [47].

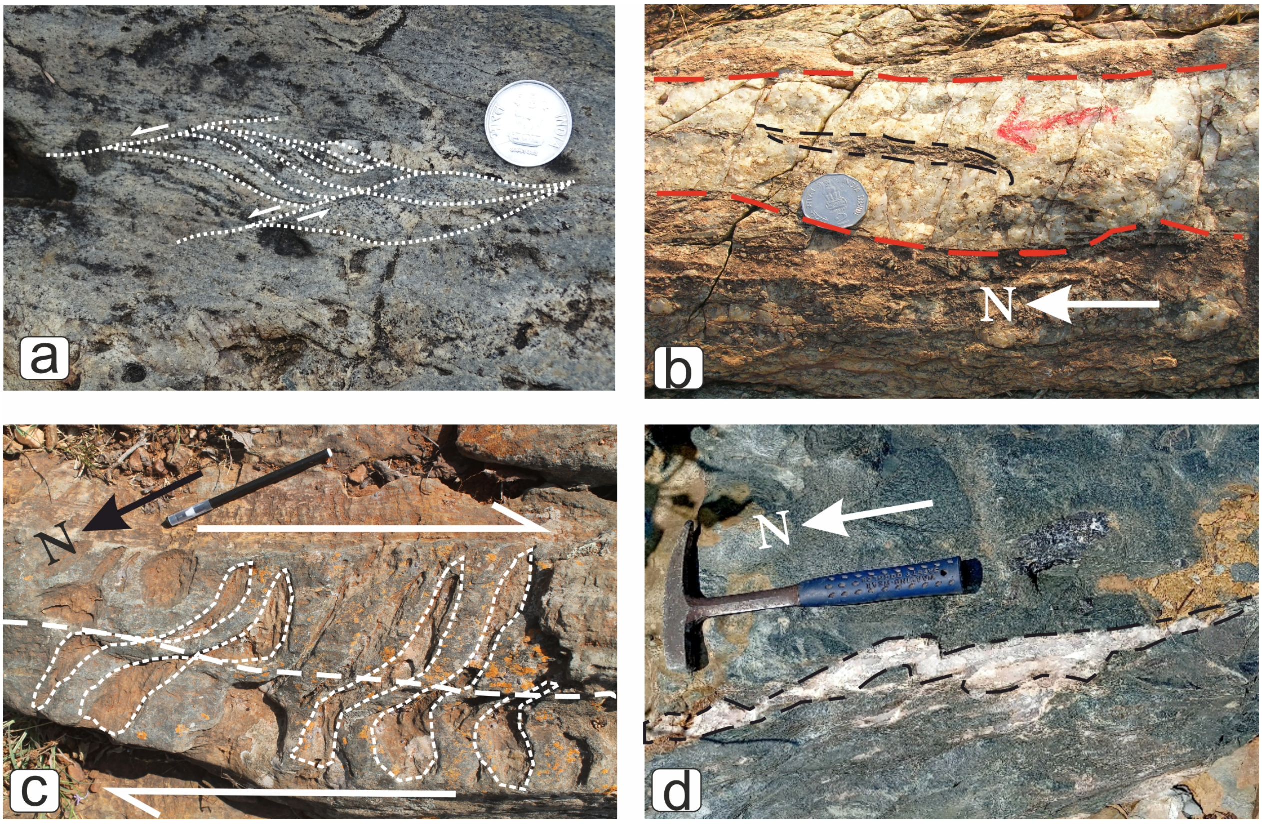

Figure 2. Field photographs showing (**a**) brittle-ductile sinistral shearing within the Champion gneiss in the Chgargunta deposit (SKGB); (**b**) N–S oriented quartz vein along the Sh_2 shear with shear fabric from Jonnagiri (JGB); (**c**) Tension gash vein in metabasalt near Nabhapur of the GGF, indicating a dextral sense of shear; (**d**) Sigmoidal quartz-carbonate veins along the shear zone in the sheared metabasalt at Paramanahalli prospect (CGB).

Guddadarangavvana Halli (G.R. Halli) gold deposit hosts auriferous quartz–sulfide lode-type mineralization within metabasalts situated along the Chitradurga Central Shear Zone (CCSZ). Ore localization is concentrated along the contact of sheared and altered metabasalts and metasedimentary units in this NNW–SSE striking shear zone, which shows significant carbonatization [48]. The importance of structurally focussed fluid flow in ore deposition is shown by the fact that gold mineralization is generally linked to quartz veins situated along faults and shear zones. Pyrite, arsenopyrite, sphalerite, galena, and minor chalcopyrite are the major sulfides in the mineralized zone. The G.R. Halli deposit is located within the CCSZ and close to the Chitradurga Boundary Shear Zone (CBSZ), according to previous studies [49, 50], mineralization is found contemporaneous with other shear-zone hosted orogenic gold deposits in the CGB.

Although the principal gold mineralization across the Dharwar Craton is closely linked to Neoarchean (ca. 2.7–2.5 Ga) tectono-metamorphic events, several deposits record evidence of younger tectono-thermal reactivation (e.g., Hutti). The Neoarchean event was characterized by regional amphibolite-facies metamorphism, crustal shortening, transpressional deformation, and the development of large-scale shear zones that channelled metamorphic fluids responsible for orogenic gold deposition. In contrast, younger Proterozoic tectono-thermal events predominantly resulted in localized brittle to brittle–ductile reactivation of pre-existing Archean structures, renewed fluid circulation, and hydrothermal alteration rather than the formation of major new gold systems. These younger events commonly caused remobilization of existing sulfides and gold, vein rejuvenation, isotopic resetting of susceptible mineral systems, and overprinting of alteration assemblages, but generally did not obliterate the fundamental Neoarchean structural and metallogenic framework. Consequently, distinguishing primary Archean mineralization from later tectono-hydrothermal modifications is critical for interpreting the evolution of the Dharwar gold systems and for developing robust exploration models. For example, localized later hydrothermal overprints are reported at Hutti. These are interpreted as limited later reactivation of pre-existing structures with no significant neo-mineralization or new quartz reef formation rather a last major hydrothermal alteration event at 2332 $\pm$ 12 Ma [51, 52]. The preservation of primary deformation fabrics, hydrothermal assemblages, and Archean mineralization ages further suggests negligible influence of younger tectono-thermal events on the genesis of these deposits.

3. Greenstone Metamorphism, Geochronology and Associated Gold Mineralization

3.1. Metamorphism

According to [13, 23], the Hutti metavolcanics within the Hutti–Maski Greenstone Belt (HMGB) indicate amphibolite–facies metamorphism, with peak *P*–*T* conditions estimated at ~5 kbar and 660 $\pm$ 40 °C. Peak metamorphic conditions at Uti also reached the middle amphibolite facies ($P = 6$ kbar; $T = 650$–700 °C). This was followed by a clockwise prograde *P*–*T*–*t* trend, which is suggestive of compressional to transpressional tectonics connected to subduction [23]. Near-isothermal decompression is a characteristic of subsequent retrograde metamorphism in HMGB, which is consistent with the emplacement of late Archean plutons and is explained by the upward transport of greenstone sequences through entrainment in ascending syn-tectonic magmas [23, 53]. On the other hand, there are still less constraints on the metamorphic history of the Kolar Gold Field (KGF). According to [54], available mineral assemblages indicate amphibolite-facies conditions at temperatures ≥500 °C. Subsequent hydrothermal overprints show decompression-dominated cooling during lower amphibolite–facies metamorphism ($P = \sim$4.6 kbar; $T = \sim$600 °C) around 2546 $\pm$ 12 Ma, from the South Kolar Greenstone Belt (SKGB) [53]. Similar to the metamorphic trajectory recorded at Uti in the HMGB, the clockwise *P*–*T* path characteristic of compressional regimes characterizes the prograde metamorphism in SKGB. The stable hornblende + plagioclase assemblage and thermobarometry showing conditions like $P = 4.6$–5.5 kbar and $T = 470$–515 °C supported by [36], detailed metamorphic analyses, which demonstrated amphibolite-facies conditions, contrasted to early interpretations that placed the Jonnagiri greenstones within the greenschist facies [34]. However, according to [36] metamorphism at Jonnagiri is constrained at at ~5 kbar and 500 °C, a lower amphibolite-grade metamorphism involving peak conditions. Metamorphism and mineralization across the WDC, characterized by high-temperature–low-pressure metamorphism, penetrative shear deformation, and enhanced fluid circulation, likely contributed to gold mineralization in G.R. Halli, Ajjanahalli, Gadag, and Paramanahalli [55, 56]. According to [57], structural controls are of primary importance for the localization of gold mineralization throughout the Dharwar Craton. Shear zones that are extensive on a regional scale and trend NNW–SSE, such as the Chitradurga, Chitradurga Central, and Kolar shear systems, acted as the main channels for metal bearing hydrothermal fluid migration. These zones facilitated concentrated fluid flow, widespread interaction between fluid and wall-rock, and effective transport of metals. As a result, significant gold deposits such as Kolar, Hutti, Ramagiri, Gadag, Ajjanahalli, G.R. Halli, and Paramanahalli are found along these structurally reactivated zones/corridors. These shear zones played a critical role in the metallogeny and evolution by enabling the rise of deep-seated metamorphic fluids and offering structural traps essential for gold deposition. The GGB records greenschist- to amphibolite-facies Barrovian metamorphism associated with progressive D_2 deformation. Mineral chemistry, geothermobarometry, and pseudosection modelling indicate peak metamorphic conditions of ~560–600 °C and ~6.5–8.5 kbar for amphibolite units, whereas garnetiferous schists preserve comparatively lower conditions of ~490–540 °C and ~5.6–7.0 kbar. Hornblende–plagioclase thermobarometry yielded temperatures of ∼577 ± 21 °C and pressures of ∼7.1–7.4 kbar, while garnet–biotite and chlorite–garnet thermometry constrains temperatures between ∼501 and 616 °C, supporting syn-tectonic prograde metamorphism during D_2 deformation and crustal thickening in the GGB [58].

3.2. Hydrothermal Alterations

Hydrothermal alteration is a key signature of gold mineralization across the Dharwar Craton and provides a important guide to fluid pathways and ore localization. Most deposits such as Kolar, Hutti, Uti, Hira-Buddini, Jonnagiri Ramagiri-Penakacherla, Gadag, G.R. Halli, Ajjanahalli, and exhibit a broadly kind of similar alteration pattern that reflects the interaction of metamorphic, CO_2-rich hydrothermal fluids with diverse host rocks under greenschist-facies conditions [32, 36, 47, 59, 60]. In the studied gold deposits in Dharwar Craton, the distinct alteration assemblages are observed. Kolar gold deposit is characterized by sericitization, carbonatization, and chloritization [61]. At Hutti, sulfidation is the dominant alteration process. Chigargunta exhibits sericitization, tourmalinization, carbonatization, and chloritization. Ajjanahalli is marked primarily by carbonatization and silicification. In Paramanahalli, the major alterations are represented by chloritization, carbonatization, silicification, and sulfidation reflecting fluid–rock interaction along the major shear zones and it's splay. A consistent distal–proximal alteration zonation is recorded in several mining camps. Distal domains are dominated by chlorite–carbonate ± albite alteration, particularly well expressed in mafic hosts at Hutti and G.R. Halli [62]. Approaching the ore zones, the assemblage transitions into sericitization and carbonatization, as documented around auriferous veins at Jonnagiri [63]. The immediate ore-proximal zone is identified by intense silicification, sericite–ankerite formation, and pervasive sulfidation (pyrite ± arsenopyrite), especially characteristic of the Hutti mine sequence [59]. At Ajjanahalli, the mineralized rocks exhibit strong carbonatization and sericitization accompanied by arsenopyrite–pyrite sulfide assemblages, indicates the focused fluid–rock interaction [44]. Alteration patterns vary with host lithology in which mafic metavolcanics generally show pervasive chlorite–carbonate–epidote alteration (Hutti, Uti), whereas BIF-hosted zones, such as in the Paramanahalli and Ajjanahalli area, display intense carbonatization. Hydrothermal alteration associated with gold mineralization in the Gadag is characterized by quartz–carbonate–muscovite–chlorite–sericite ± tourmaline assemblages with pyrite, arsenopyrite, chalcopyrite ± sphalerite. Two stages of hydrothermal alteration and mineralization have been recognized, both linked to progressive D_3 deformation with dextral shearing. Stage-I alteration is characterized by carbonate-dominated assemblages containing euhedral to subhedral pyrite with subordinate quartz and muscovite alteration, which was subsequently overprinted by a Stage-II sulfide-rich alteration assemblage comprising muscovite + sericite + chlorite + carbonate + quartz ± tourmaline [31, 42]. In the Ramagiri–Penakacherla belt, quartz-chlorite schists undergo progressive sericitization, silicification and sulfidation along shear cores, consistent with fluid infiltration during deformation [64]. Overall, hydrothermal alteration assemblages in the Dharwar Craton not only record the physicochemical evolution of the ore-forming fluid but also serve as powerful exploration tool.

3.3. Geochronology

The mafic volcanic rocks of the Hutti greenstone belt yield a Sm–Nd whole-rock age of 2662 ± 81 Ma [65, 66], whereas the associated felsic volcanics record a U–Pb zircon age of 2587 ± 7 Ma [55]. Broader geochronological synthesis by [11], based on U–Pb zircon dating using SIMS from seven EDC greenstone belts, indicates a bimodal magmatic accretion history with two major episodes: (i) emplacement of juvenile tonalite–granodiorite suites between 2700–2650 Ma, synchronous with mafic volcanism, and (ii) felsic volcanism between 2580–2540 Ma, coeval with calc-alkaline magmatic activity in the EDC. Comparable ages are documented for granitoids spatially associated with the Hutti–Maski greenstone belt: the Kavital granitoid records U–Pb zircon ages of 2543 ± 9 Ma [16] and 2545 ± 7 Ma [55], while the Yellagatti granitoid crystallized at 2532 ± 3 Ma based on U–Pb titanite geochronology [65, 66]. Hydrothermal monazite linked to Stage-1 mineralization at Hutti yields a “preferred age” of 2547 ± 10 Ma [55]. The maximum sedimentation age of the HMGB is constrained by the $^{207}Pb/^{206}Pb$ zircon age of 2576 ± 12 Ma from a granitoid pebble in the Palkanmardi conglomerate [67]. Monazite grains from volcaniclastic and intermediate units of the HMGB and SKGB give ages of 2564 ± 12 Ma and 2546 ± 12 Ma, respectively, representing metamorphic overprints [53]. In the western EDC, felsic volcanics of the Ramagiri belt yield a U–Pb zircon age of 2707 ± 18 Ma, whereas titanite in nearby granitoids records a poorly constrained Pb–Pb age of 2614 ± 18 Ma [68]. U–Pb zircon dating of granitoids near the Kolar deposit provides crystallization ages of 2610 ± 10 Ma for the Dosa granite and 2551 ± 2.5 Ma for the Patna granite [69]. The basic metavolcanics of the Kolar sequence also yield Pb–Pb zircon ages of 2732 ± 155 Ma [70].

In situ zircon U–Pb geochronology [71] indicates that the felsic metavolcanics, Pagadarayi granodiorite, and Chennampalli granite crystallized at 2690 ± 17 Ma, 2651 ± 14 Ma, and 2557 ± 10 Ma, respectively. These ages correlate well with published radiometric data from auriferous greenstone–granite terranes of the Dharwar Craton. A detailed comparative account of the geochronology of the Jonnagiri rocks is provided by [36]. Although the precise timing of mineralization remains uncertain, comparison with mineralization ages reported elsewhere in the Dharwar Craton suggests a likely emplacement at ∼2545 Ma, postdating the intrusion of late-stage granite–syenogranite batholiths. Zircon U–Pb dating by LA-ICP-MS further constrains the magmatic evolution, with the Pagadarayi granodiorite yielding a concordant emplacement age of 2651 ± 14 Ma, while the Chennampalli granite records concordant ages of 2557 ± 10 Ma and 2532 ± 22 Ma.

Within the WDC, the felsic volcanics of the Gadag greenstone belt record a U–Pb zircon age of 2588 ± 10 Ma [63], and surrounding granitoids crystallized around ∼2560 Ma [72]. A SHRIMP U–Pb zircon age of 2547 ± 5 Ma from turbidite greywacke constrains the maximum sedimentation age for the CGB greenstones [73]. Hydrothermal xenotime records gold-mineralization ages of 2522 ± 6 Ma at Gadag and 2520 ± 9 Ma at Ajjanahalli [63].

Gold mineralization in the Dharwar Craton occurred between 2547 and 2510 Ma, as indicated by integrated geochronological datasets [74]. This period includes deposits such as Kolar (2546 ± 12 Ma), Hutti (2547 ± 10 Ma), Ajjanahalli (2520 ± 9 Ma), Gadag (2522 ± 6 Ma), and Paramanahalli (2510 ± 12 Ma). The observed temporal clustering indicates a potentially extensive gold-mineralizing event at the craton wide scale. Nevertheless, the differences between EDC and WDC ages suggest the possibility of several distinct mineralization episodes instead of single major cratonic event. Despite thorough geochronological studies, is inadequate for fully clarifying the ongoing debate regarding the origin of mineralizing fluids. Competing models propose either (i) fluids exsolved from *syn*-tectonic magmatic intrusions, or (ii) metamorphic devolatilization of greenstone sequences. Thus, the age of ∼2520 Ma of the gold mineralization in Ajjanahalli, Gadag, and Paramanahalli deposits is because the flow of circulation of large-scale metal-rich hydrothermal along major shear zones during late Neoarchean tectonothermal events. A holistic summary with detailed timeline of tectono-thermal events that occurred in the Dharwar Craton in relation to gold mineralization is presented in Figure 3 and also presented in Table 1.

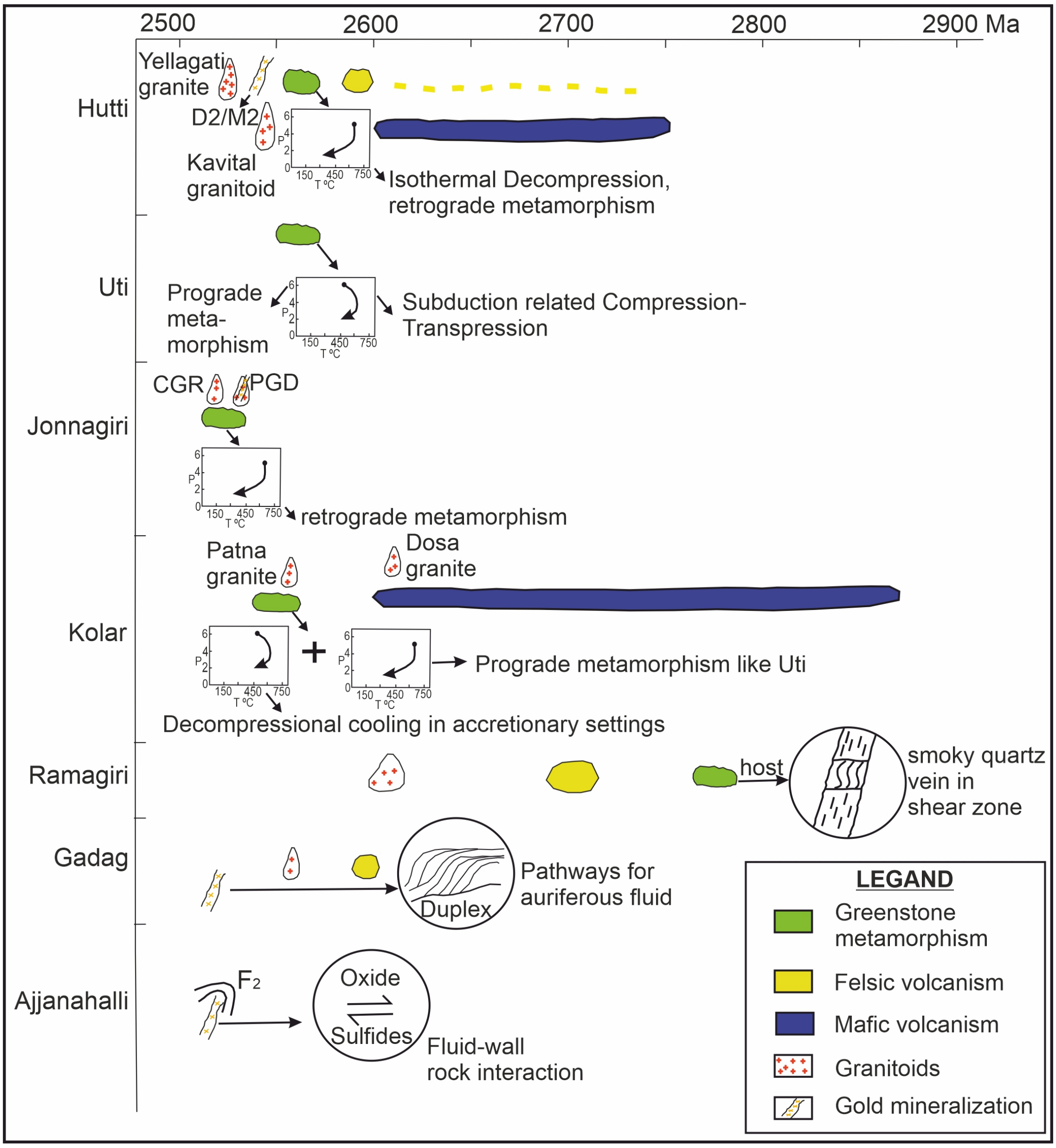

Figure 3. Time and space relationship of tectono-thermal events such as bimodal volcanism, greenstone metamorphism, magmatism, and gold mineralization from different deposits/prospects of Dharwar craton.

Table 1. Summary of the characteristic genetic features of orogenic gold fields/deposits/prospects and associated greenstone belts terranes in the Dharwar craton.

Greenstone belts	Gold fields	Host rock	Age of mineralization/hydrothermal alteration	Age of metamorphism (Ma)	Metamorphic *P* (kbar)/*T* (°C) conditions	Alteration mineral assemblages	Ore mineral assemblages	Salinity (wt% NaCl equiv.)/ Ore fluid composition	*P* (kbar)/*T* (°C) conditions	Inferred fluid source(s)
HMGB	Hutti	Felsic Volcanics (FV), Metabasalt (MB)	2547 ± 10 [55]	NA	3–5/∼650 [15, 23] ∼5/600–685 [75] 4/660 ± 40 [13]	Bt + Chl + Act + Tur + Cal + Qz ± Ms [15, 23] Chl + Cal + Ep + Qz + Spn [51] Qz + Ser + Cal + Bt + Or + Ab [51]	Apy + Py + Po + Ilm + Sp [23, 75] Apy + Py + Po + Ccp + Ilm + Sp + Sch [51]	1.7–6.7/H_2O–CO_2–NaCl ± CH_4 (Stage-1) [75] 3.9–13.5/ H_2O–CO_2–NaCl (Stage-2) [75] 2–8/H_2O–CO_2–NaCl (Stage-2) [51]	1.0–3.0/350–480 (Stage-1) [75] 1.0–1.7 / 280–320 (Stage-2) [75] 1.6–3.6/240–360 [51]	Early deep-seated metamorphic fluid (Stage-1) [15] Mixing of magmatic and light formation fluid (Stage-2) [13] Metamorphic fluid [53, 59, 75, 76] Average crustal fluid source [37]
	Hira-Buddini	Felsic Volcanics (FV), Metabasalt (MB)	NA	NA	NA	Bt + Tur + Cal + Chl + Qz [60] Bt + Kfs + Act + Ab + Tur + cal + Qz (MB) [23, 60, 77] Ms + Cal + Chl + Ab + Bt + Qz (FV) [60]	Py + Po + Ccp ± Gn ± Sp [60] Py + Ccp ± Po ± Sch ± Ilm [23, 77]	Low saline / H_2O–CO_2–CH_4–NaCl [23]	2.05–4.36 / ∼500 [60] 550 [77]	Average crustal fluid source [78] Magmatic fluid followed by a fluid of metamorphic origin [53, 77]
	Uti	Metabasalt	2414 ± 18 [79]	2564 ± 12 [80]	∼6 / 650–700 [23] ∼6 / ∼620 [80]	Qz + Kfs + Pl + Bt + Act + Spn [12]	Py + Apy + Po + Lo ± Ccp ± Sp [12]	Two stage low and high saline / H_2O–NaCl [12]	3–4 / 400–450 [12]	Average crustal fluid source [78]
RPB	Ramagiri	Phyllite				Ser + Chl + Qz + Cb [81]	Py ± Ccp [81, 82]	Low saline / CO_2 ± NaCl [81] Both Low and High saline / H_2O + CO_2 + CH_4 + CO_2 [82]	1.45–1.7 / 240–267 [75]	Diverse source including granite and metamorphogenic fluid [82]
KGB	Kolar	Champion gneiss, Metabasalt			Amphibolite facies [54]	Qz + Bt + Ep + Chl ± Cal [83]	Po + Py + Apy + Sch ± Ccp ± Gn ± Sp [61]	∼7 / H_2O–CO_2–NaCl [83] Both low and high saline fluid (Sulfide rich lode) [83] ∼3–12 / H_2O–CO_2–NaCl [61]	0.7–1.8 / 205–280 [83] 290–420 [61]	CO_2 rich metamorphic fluid [61] Magmatic as well as metamorphic fluids [32, 42]
SKGB	CG	Champion gneiss	2414 ± 26 [80]	2546 ± 12 [80]	∼4.6 / ∼600 [80]	Chl + Bt + Ms + Tur + Ep + Ser + Qz ± Cal [32]	Po + Py + Apy + Ccp + Ilm [32]	0.5–13.3 / H_2O–NaCl–CO_2–CH_4 ± N_2 [32]	1.7–3.5 / 285–378 [32]	Metamorphic fluid [32]
	BN	Metabasalt				Chl + Bt + Ms + Tur + Ep + Ser + Qz ± Cal [32]	Apy + Po + Py ± Mol [32]	01.6–6.4 / H_2O–NaCl [32]	0.8–1.2 / 365–405 [32]	
JGB	Jonnagiri	Granitoid	NA	NA	∼6 / ∼620 [36]	Ms + Pl + Chl + Qz + Ab + Ep + Cal ± bt [35]	Py + Po ± Apy ± Ccp ± Ilm ± Rt [35]	∼5 / H_2O–NaCl–CO_2 ± CH_4 [35]	1.4–2.5 / 263–323 [80]	Average crustal fluid source [78]
GGB	GGF	Metabasalt, Argillite, BIF	2522 ± 6 [63]	2547 ± 5 [73]	NA	Qz + Ank + Chl + Ser [40] Qz + Tur + Ank + Chl + Ms + Ser	Apy + Py + Po + Ccp ± Sp ± Gn ± Sch [40] Apy + Py + Ccp	5–10 / H_2O–NaCl–CO_2 ± CH_4 fluid [84] 2.0–6.6 / H_2O–NaCl–CO_2 [85] 0.04–9.6 / H_2O–NaCl–CO_2 ± CH_4	∼1 / 216–321 [84] 175–325 [85] 1.6–2.9 / 296–333	Magmatic and/or Mantle source [84] Metamorphic fluid [42]
CGB	Ajjanahalli	BIF	2520 ± 9 [63]	NA	NA	Chl + Qz + Cal + Ank + Ser [13, 44]	Po + Asp + Po + Ccp + Sp [13, 44]	Low saline / H_2O–CO_2–NaCl ± CH_4 [44]	0.8–1.2 / 265–310 [44] 300–350 [13]	Juvenile granitic fluid [13, 56] Average crustal fluid source [78]

3.4. Fluid Inclusions Studies

Gold deposits across the Dharwar Craton are characterized by broadly similar aqueous–carbonic ore fluids, with notable exceptions at Uti and in the sulfide-rich lodes of the Kolar deposit. At Hutti, Stage-1 mineralization was produced by a low-saline aqueous–gaseous fluid (H_2O–CO_2–NaCl ± CH_4; 1.7–6.7 wt% NaCl equiv.) that precipitated gold along a retrograde path through fluid–wallrock sulfidation under P = 1.0–3.0 kbar and T = 350–480 °C [75]. Stage-2 fluids, trapped within laminated quartz veins and associated K-feldspar–chlorite, record broadly similar pressures (1.0–3.6 kbar) but lower temperatures (240–360 °C) and consist of mixed CO_2–H_2O–NaCl fluids with 3.9–13.5 wt% NaCl equiv. [51, 75]. Phase separation triggered by sudden pressure drops destabilized $Au(HS)_{2-}$ complexes, facilitating gold deposition [23, 51] distinguished five fluid-inclusion types at Hutti CO_2-rich monophase inclusions, low-salinity aqueous biphase inclusions, low-salinity CO_2–H_2O inclusions, high-salinity polyphase inclusions with nahcolite ± halite, and polyphase aqueous inclusions with halite/sylvite assemblages which collectively record progressive depressurization and fluid immiscibility within a CO_2–H_2O–NaCl system. A similar mechanism is documented at Hira-Buddini, where an initial CO_2–H_2O–NaCl–CH_4 fluid underwent pressure-controlled phase separation due to fault-valve behaviour in steep fault-fill and sigmoidal extension veins, reducing sulfur activity and precipitating gold [23]. In contrast, the amphibolite-hosted Uti deposit preserves two distinct aqueous H_2O–NaCl fluids a low-salinity (∼3 wt% NaCl equiv.) fluid responsible for gold deposition at 3–4 kbar and >400 °C, interpreted as meteoric water, and a later high-salinity (up to 22 wt% NaCl equiv.) granite-related fluid that participated only in post-mineralization mixing [12]. The extremely low CO_2 content ($XCO_2 \leq 0.02$) at Uti is unusual within the craton and reflects its structural and lithological proximity to the Kavital and Yellagatti granitoids.

In the EDC, dominantly carbonic inclusions with minor aqueous–saline inclusions characterize the Ramagiri deposit [79]. Gold precipitation occurred at 1.4–1.7 kbar and 240–267 °C from an aqueous–carbonic fluid with variable salinity and CH_4 content. High-saline, CO_2–H_2O–NaCl–CH_4 inclusions likely reflect granitic input [39, 81, 82]. At the Kolar camp, the Champion lode preserves metamorphogenic H_2O–CO_2–NaCl fluids that underwent pressure-induced immiscibility, precipitating gold at 0.7–1.8 kbar and 205–280 °C. In contrast, the sulfide-rich McTaggart and Oriental lodes contain no carbonic inclusions, consistent with mixing between low-salinity meteoric fluids (≤7 wt% NaCl equiv. ≤200 °C) and high-salinity, high-temperature (≥50 wt% NaCl equiv. ≥400 °C) magmatic fluids [83]. As per [61] documented low-saline, H_2O–CO_2–NaCl fluids (3–12 wt% NaCl equiv.) and CO_2-rich metamorphic fluids as plausible fluid sources for parts of the Kolar gold field. Studies from Chigargunta and Bisanatham record primary H_2O–CO_2–NaCl–CH_4 ± N_2 inclusions (0.5–13.3 wt% NaCl equiv.) and demonstrate fluid immiscibility and wall-rock interaction at a wide range of P–T conditions of 1.7–3.5 kbar / 285–378 °C (CG) and 0.8–1.2 kbar / 365–405 °C (BN), responsible for gold deposition [32, 33]. The granitoid-hosted, Jonnagiri deposit contains primary, secondary, and pseudo-secondary inclusions in both auriferous and proximal alteration zones [35]. Gold was precipitated from a metamorphogenic H_2O–CO_2–CH_4–NaCl fluid via (i) destabilization of $Au(HS)_{2-}$ during fluid–wall-rock interaction and (ii) pressure-induced, CH_4-related expansion of the H_2O–CO_2–NaCl solvus [86], under 1.4–2.5 kbar and 263–323 °C [35, 36].

In the WDC, the Ajjanahalli deposit formed through an initial metamorphogenic H_2O–CO_2–CH_4–NaCl fluid that was focused during D_2 deformation of BIF units and underwent near-isothermal decompression [44]. This led to aqueous–carbonic immiscibility at 0.8–1.15 kbar and 263–309 °C, enabling the low-salinity aqueous phase to react with iron oxides, generating sulfides and coeval gold precipitation [44]. At Gadag, three fluid-inclusion types are recognized [85]. Dominantly aqueous–carbonic fluids (0.4–9.6 wt% NaCl equiv.; ∼30 mol% CO_2) precipitated gold between 175–325 °C under reducing conditions. Progressive carbonitization of wall rocks promoted phase separation, producing CH_4 bearing, less CO_2-rich fluids. The Paramanahalli deposit recods similar physico-chemical conditions, with gold deposition at P–T of ∼2.2 kbar and ∼330 °C from a low- to moderately saline (up to ∼12 wt% NaCl equiv.), CO_2-rich aqueous fluid similar to other metamorphic-sourced fluid [87]. Across the craton, the prevailing ore fluids such as low-saline, aqueous–carbonic, H_2O–CO_2–NaCl ± CH_4 rich fluid is remarkably uniform. The absence of carbonic inclusions at Uti reflects its distinct fluid regime associated with granite-proximal hydrothermal processes, whereas carbonic depletion in the McTaggart and Oriental lodes at Kolar records a contrasting fluid-mixing pathway from different crustal reservoirs [12, 83].

3.5. Stable Isotopes

According to [15] the calculated $\delta^{18}O$ = 7.3‰ and δD = −61‰ values are for amphibolite host rocks and $\delta^{18}O$ = 7.5‰ and δD = 51‰ for associated felsic volcanics occurring at Hutti in HMGB. While biotite-plagioclase alteration zone, proximal to stage-1 quartz vein at Hutti, yielded whole rock $\delta^{18}O$ = 6.8‰ and δD = −60‰. The whole rock isotopic ratios for distal chlorite-biotite alteration zone of the same stage recorded $\delta^{18}O$ = 6.2‰ and δD = −56‰ implying both the alteration zones have similar δD values to that of unaltered host rock and $\delta^{18}O$ values show a decreasing trend from unaltered to altered host rocks. The authors also suggested slightly heavier $\delta^{18}O_{fluid}$ = 7.8 to 7.9‰ and lighter δD_{fluid} = −26 to −29‰ fluid isotopic composition for biotite-plagioclase alteration zone as compared chlorite-biotite alteration zone, that is having $\delta^{18}O_{fluid}$ = 7.5‰ and δD_{fluid} = −23‰. In stage-2 mineralization at Hutti, $\delta^{18}O_{fluid}$ values for laminated, milky and grey quartz veins are around 6.8‰ and those for the fluid that equilibrated with scheelite are around 3.6‰. The fluid isotopic value associated with inner chlorite-K-feldspar alteration zone ranges from 2.3 to 5‰ for $\delta^{18}O_{fluid}$ and −23 to 32‰ for δD_{fluid}. On this basis, the authors argued that deep seated metamorphic fluid of higher $\delta^{18}O_{fluid}$ values may have mixed with formation water of lighter $\delta^{18}O_{fluid}$ values during fluid wall rock interaction. In contradiction to above discussion for Hutti mineralization, analogous tourmaline composition for both the stages from Hutti was suggested by [76, 80]. Quartz vein from ore zone within greenstone pile and quartz/pegmatitic veins from granite domain in RPGB recorded $\delta^{18}O$ values in the range 10.4 to 14.9‰ and 9.3 to 10.9‰ respectively. The oxygen isotopic ratio of ore fluid at 1 kbar at Ramagiri and Penakacherla reflects 7.9 ± 1.5‰ and 5.1 ± 0.8‰ respectively. Which is higher as compared to $\delta^{18}O_{fluid}$ values (4.5 ± 0.7 at 1 kbar) for granitoid derived late magmatic fluid. The plausible cause of increase of $\delta^{18}O_{fluid}$ values in greenstone sequences compared to that in granite domain is due to interaction of the fluid with greenstone pile after magmatic origin in the RPGB [39]. The authors suggested that the fluid derived from granitoids emplaced in mid crustal level around 14 to 19 km depth under *P*–*T* conditions of 4.2–5.7 kbar and 650–750 °C, based on oxygen isotope data in conjunction with fluid inclusions results of [82]. However, there is possibility of making interpretation on ore forming fluid based on observations made on non-mineralizing fluid because all the data obtained are from surface samples without having access to the subsurface drill cores/mines. In structurally controlled hydrothermal deposit, it is necessary to establish vein chronology where the mineralized and hydrothermally altered higher order splays required to be separated from first order and barren splays through careful examination of subsurface samples [5, 88]. Again, granitophilic suite of elements commonly associated with such magmatic intrusion related type of deposit [89–91]. Sulfur isotope systematics from Dharwar Craton gold deposits provide an important constraint on the relationship between sulfur, gold, and ore fluid source. Early sulfur isotope investigations from the Dharwar Craton include studies on the Hutti gold deposit [92] and Ajjanahalli gold deposit [13], which demonstrated relatively restricted sulfur isotope compositions in ore-associated sulfides. Subsequently, a craton-scale sulfur isotope study by [78] showed that sulfides associated with auriferous quartz–carbonate veins, particularly pyrite and arsenopyrite, display a relatively narrow $\delta^{34}S$ range (ca. +1 to +7‰) across major deposits such as Hutti, Hira-Buddini, Uti, Kolar, Ajjanahalli, and Jonnagiri, with average value 4.2‰, suggesting a broadly homogeneous sulfur reservoir in the Dharwar Craton. The authors further reported crustal scale consistency of ore fluid sulfur isotopic compositions, $\delta^{34}S_{H_2S}$ in many deposits of Dharwar Craton, which ranges in 2.5–4.5‰, 2.1–5.2‰, 0.2–5.8‰ and 2.0–3.4‰ for Hutti stage-1, Hira-Buddini, Jonnagiri and Ajjanahalli camps respectively characterizing ore fluid of orogenic gold deposit (Figure 4). Similar and overlapping ranges of $\delta^{34}S$ isotopic data between mineralized sulfide grains (+1.5 to +4.5‰) and host rock pyrites (−1 to +3.8‰) of the Gadag Gold Field (GGF), suggest the dissolution of preexisting magmatic and metasedimentary pyrites of the host rocks during high fluid flux contributed most of the sulfur in the hydrothermal system [42]. Ore fluid sulfur ($\delta^{34}S_{H_2S}$) isotopic composition, derived from $\delta^{34}S$ values of sulfides, varies from −0.42 to +2.43‰ and +0.25 to +2.34‰ for Chigargunta and Bisanatham respectively [32]. Such a narrow range of ore fluid sulfur isotopic composition is interpreted by [78] in support of [93], as sulfur derived from (1) homogeneous magmatic source either directly exsolved by magma or remobilization from magmatic rocks and (2) crustal source. Though Mass Dependent Fractionated Sulfur (MDFS) isotope signatures have some limitations in inferring the source of sulfur in ore fluid, Ref. [94] inferred crustal source of sulfur in many deposits from Yilgarn Craton, Western Australia except few giant ones like Charlotte-Golden Mile, based on Mass Independent Fractionated Sulfur (MIFS) isotope signatures of samples from 24 deposits of the Craton. With the aid of these observations, the narrow variation of $\delta^{34}S_{H_2S}$ without negative values in Dharwar Craton (Figure 4) can be inferred as assimilation of crustal sulfur during advection of ore fluid and sulfide precipitation from reduced fluid below H_2S–HSO_4 boundary [36, 78]. Narrow isotopic range of ore fluid oxygen isotopic compositions, $\delta^{18}O = 6.5$–8.5‰ and initial $^{87}Sr/^{86}Sr = 0.7068$–0.7078 in BIF hosted Ajjanahalli deposit implying a mineralizing fluid generated from metamorphic devolatilization of deeper Chitradurga greenstones sequences [57]. Carbonates and fluids $\delta^{13}C$ values in Quartz Carbonate Veins (QCV) for Ajjanahalli range −5.5 ± 1.3‰ and −5.81 ± 1.14‰ respectively and those for G.R. Halli fall in the range −6.2 ± 1.9‰ and −4.64 ± 0.7‰ respectively which are not enriched compared to BIFs and metavolcanics of Chitradurga Group with $\delta^{13}C$ values range 0 ± 2‰ [56]. At Ajjanahalli, $\delta^{18}O$ of carbonates fall in the range of 11.41–18.97‰ and fluid $\delta^{18}O$ fall in the range 6.88–20.16‰ in QCV. Similarly, $\delta^{18}O$ values for carbonates and fluid at G.R. Halli deposit fall in the range of 12.87–14.89‰ and 5.84–7.27‰ respectively. Dissolution and decarbonation reactions during metamorphism produce CO_2 with $\delta^{13}C$ values similar or more enriched than in parent rock [95, 96]. On the basis of this, Ref. [56], argued a juvenile granitic or mantle source for auriferous fluid at Ajjanahalli and G.R. Halli as the values of $\delta^{13}C$ in QCV in both the camps are not enriched compared to corresponding values in BIFs and metavolcanics rocks. The carbonate and fluid $\delta^{13}C$ values of auriferous QCVs of the Ajjanahalli and G.R. Halli gold deposits in the Dharwar Craton point to magmatic/mantle source for the mineralizing fluids [56]. Ref. [84], estimated $\delta^{13}C$ and $\delta^{18}O$ of QCV from different mines of GGF. $\delta^{13}C$ values for carbonate ranges from −2.2 to −9.7‰ and fluid $\delta^{13}C$ ranges from −2.1 to 9.6‰. According to [42], carbon isotope compositions from hydrothermal carbonates at GGF indicate calculated ore-fluid values of $\delta^{13}C_{fluid}$ ranging from approximately −6.0 to +1.5‰, suggesting derivation from a relatively homogeneous and isotopically buffered carbon reservoir. These values are interpreted to reflect interaction with carbonate-bearing lithologies and/or contribution from a deep-seated metamorphic fluid system. Corresponding estimated values of $\delta^{18}O$ for carbonates and fluid ranges from 12.0 to 30.0‰ and 6.8–25.9‰ respectively. The authors in an analogous argument like [56], for Ajjanahalli and G.R. Halli, suggested magmatic or mantle source for auriferous fluid in GGF which got emplaced in crustal level shear zones in WDC. But the aforementioned oxygen isotopic ratios are very wide in contrast to narrow well constrained isotopic range ($\delta^{18}O = 6.0–11.0‰$) suggested by [88], for orogenic ore forming fluid. Moreover, carbon isotopic compositions of carbonates perform as tracers of carbon instead of ore fluid [88].

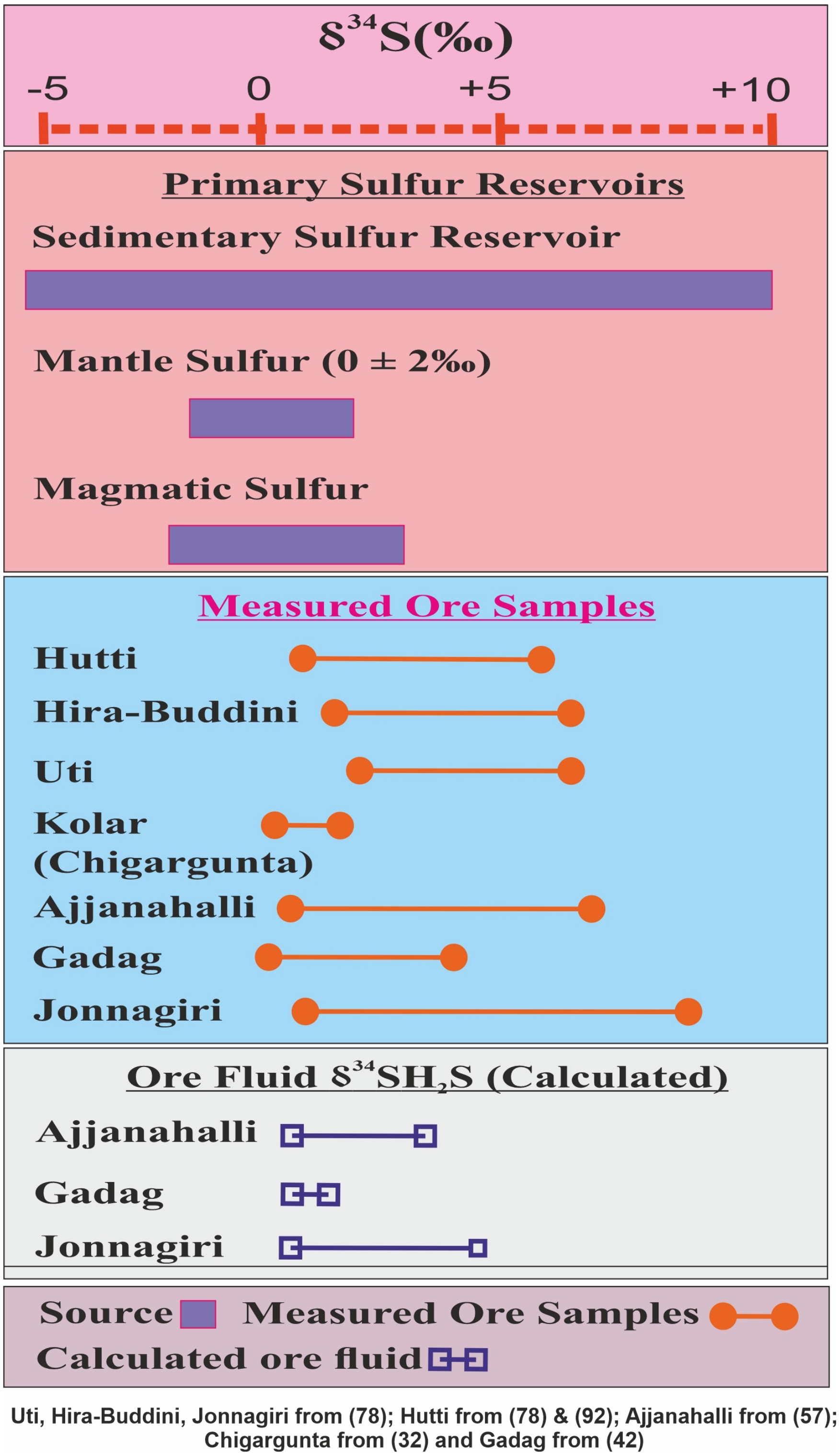

Figure 4. Sulfur isotopic data available from the gold deposits/prospects in the DC compared with magmatic sedimentary and mantle sulfur values.

3.6. Geochemistry of Accessory Phases Associated with Mineralization

The characteristic of ore forming fluid, hydrothermal fluid evolution, and mineralizing processes can be obtained from the geochemistry of accessory minerals form ore zones especially pyrite, arsenopyrite, scheelite, tourmaline, titanite, and apatite. Due to its resistance to weathering, ability to maintain primary compositions, and ability to equilibrate with a variety of fluid chemistry tourmaline stands out among these as a particularly reliable recorder of hydrothermal conditions [97–99]. As per [77], two tourmaline generations at Hira-Buddini in EDC: (i) older anhedral grains forming clusters in wall rocks and (ii) younger monomineralic veins and quartz–albite–tourmaline veins inside the alteration zones. The isotopically lighter metamorphic fluid from greenstone devolatilization and the heavier B-rich granitic fluid are the two different fluid sources determined by boron isotope compositions. Additionally, Ref. [80] showed that early hydrothermal tourmaline follows the oxydravite–provondraite (OP) compositional trend, which is marked by high Fe^{3+}/Fe^{2+} ratios and higher Na, indicating a high-saline granitic component. Fluid mixing is suggested by deviations from the OP trend, but low-salinity developed hydrothermal fluids are represented by the most recent generation of tourmaline. Tourmalines linked to Stage-1 and Stage-2 gold mineralization at Hutti have low Na, low Fe^{3+}/Fe^{2+}, and high Al concentrations, following the dravite–foitite trend. These compositions suggest metamorphic fluids with reduced nature [76, 80]. As per minerology of ore zones, pyrite and arsenopyrite are refractory minerals that consistently maintain chemical differences linked to different ore fluids [100–102]. These sulfides from Hutti and Hira-Buddini have different fluid chemistries, according to studies [60, 103]. In contrast to Hutti (Stages 1 and 2), which has extensive arsenopyrite and As-rich pyrite (390–9353 ppm), Hira-Buddini is noticeably low in arsenopyrite, with pyrite holding just 263–863 ppm As. This indicates fundamentally different arsenic availability in ore-forming fluids. The cause of oscillatory zoning in As and Co in pyrite and arsenopyrite has been identified as an episodic influx of fluid related to a fault-valve mechanism. *In situ* trace-element investigation into texturally different pyrites at Jonnagiri [104] show that gold-bearing fluids evolved through different deformation events.

Tourmaline associated with mineralization at Gadag is dominantly alkali-group dravitic to oxy-dravitic in composition and occurs within hydrothermally altered metabasalts. The tourmalines are characterized by moderate Na contents (average $\sim$0.68 apfu), low Fe^{3+}/Fe^{2+} ratios, and Fe–Mg systematics indicative of reduced, low-salinity hydrothermal fluids. Their chemistry suggests precipitation during fluid–rock interaction, where Fe partitioning into coexisting chlorite and sulfides occurred under reduced metamorphic-hydrothermal conditions, thereby supporting a predominantly metamorphic origin of the ore fluid [42]. Compositionally zoned tourmaline in quartz-carbonate veins and unzoned tourmaline within altered metabasalt are observed [50] in G.R. Halli in WDC. They attributed these features to B-metasomatism during the emplacement of the 2.61 Ga Chitradurga granite. Additionally, these authors connected hydrothermal fluids generated during 2.56–2.50 Ga magmatic accretion in an arc-related context to tourmalinization and concomitant gold mineralization. Thus, the authors suggested that a complex hydrothermal fluid, has structural overprint on mineralization was caused by shearing-induced dissolution-reprecipitation and trace-element remobilization leads to the gold enrichment in the mineralized zones.

4. Discussion

4.1. Tectonic Evolution and Gold Mineralization in Dharwar Craton

Archean lode-gold systems worldwide are characteristic of granite–greenstone terranes, where structurally controlled higher-order splays host mineralization in different lithologies, including mafic–felsic greenstones, volcaniclastic rocks, banded iron formations, and granitoids [4, 5]. The Dharwar Craton, a complex Archean granite-greenstone terrane, records a protracted history of bimodal volcanism, sedimentation, metamorphism and significant orogenic gold mineralization [59, 104]. Despite the extensive study, the primary source of auriferous fluids whether derived from granitic magmas or from metamorphic devolatilization of greenstone sequences remains unresolved sustaining the longstanding debate on fluid source [105]. Gold mineralization in the Dharwar Craton is distributed across the major crustal blocks and exhibits close spatial association with greenstone belts, that are occurring with older TTGs, younger transitional TTGs, potassic plutons, sanukitoids, and anatectic granites (Figure 5). Ref. [103] proposed a multi-stage Neoarchean crustal evolution in which (i) TTGs formed by slab melting between 3450–3000 Ma, (ii) deeper crustal melting around 2700 Ma enriched the overlying mantle wedge, generating transitional TTGs, and (iii) slab break-off and subsequent mantle upwelling triggered low-degree melting (10–15%) of enriched mantle to produce the 2600–2560 Ma sanukitoids. Heat released during these intrusions drove crustal reworking, high-temperature metamorphism, and eventual cratonization. A very recent review work by [105], based on the geophysical, geochemical, and geochronological data, also proposed a three-stage evolution driven by westward flat-slab subduction (Figure 5a). Stage 1 (Extensional Phase), east-to-west low-angle subduction generated eastward-deepening ensialic half-graben basins that acted as depocentres for bimodal volcanism, dominated by tholeiitic Fe-rich basalts, as well as clastic and chemical sedimentation, including conglomerates, greywackes, and banded iron formations. Stage 2 (Contractional Phase) was marked by continued subduction that caused basin shortening and inversion, resulting in the development of west-verging fold-thrust belts, tight to isoclinal folding, and crustal thickening. This compressional regime was accompanied by the emplacement of juvenile granitoids as tabular intrusions along regional shear zones, supplying heat and volatile-rich fluids to the evolving crust. In Stage 3 (Oblique Subduction and Gold Mineralization), the subduction geometry shifted to an oblique SE–NW orientation, transforming the tectonic regime from predominantly thrust-dominated deformation to sinistral transcurrent shearing. Reactivation of existing structures produced N–S to NNW-trending sinistral shear corridors and associated tensile fractures that acted as fluid conduits. Repeated fault-valve cycles facilitated the rapid ascent and episodic release of mixed hydrothermal fluids into structurally favourable sites, ultimately leading to the precipitation of gold and associated sulfide mineralization.

4.2. Timing and P–T–X Conditions of Ore Forming Fluid

Based on the all-available geochronological data, syntheses in this work (Figure 4), utilizing U–Pb, Pb–Pb, and Sm–Nd isotopic data reveal two major magmatic accretion episodes in the EDC, followed by a widespread, structurally controlled gold mineralization event that spanned from 2547 to 2510 Ma across both the Eastern and Western cratonic blocks.

The first tectono-magmatic episode in the EDC is broadly defined as the primary accretion phase occurred between 2700 and 2650 Ma, marked by the emplacement of juvenile tonalite–granodiorite suites and synchronous mafic volcanism (Figure 5b). During this period, basic metavolcanics in the Kolar sequence formed (2732 ± 155 Ma), followed by felsic volcanism in the Ramagiri (2707 ± 18 Ma) and Jonnagiri (2690 ± 17 Ma) greenstone belts. Mafic volcanic rocks in the Hutti belt crystallized at 2662 ± 81 Ma, chronologically aligning with the intrusion of the Pagadarayi granodiorite (2651 ± 14 Ma).

A second prominent bimodal magmatic phase occurred between 2580 and 2540 Ma, characterized by widespread felsic volcanism and coeval calc-alkaline magmatism. During this window, felsic volcanics erupted in both the Western Dharwar Craton (WDC) at Gadag (2588 ± 10 Ma) and the EDC at Hutti (2587 ± 7 Ma). This was closely followed by extensive late-stage granitoid intrusions, including the Chennampalli (2557 ± 10 Ma), Patna (2551 ± 2.5 Ma), Kavital (2545 ± 7 Ma), and Yellagatti (2532 ± 3 Ma) granitoids (Figure 5c).

The Dharwar Craton hosts a world-class metallogenic province, with extensive gold mineralization driven by the circulation of metal-rich hydrothermal fluids along major shear zones (Figure 5c). Integrated geochronological datasets of hydrothermal minerals—such as monazite and xenotime constrain this craton-wide mineralizing event to a window between 2547 and 2510 Ma. However, the timing reveals a spatial and temporal progression in a narrow time span, rather than a single uniform event. Early-stage mineralization is largely concentrated in the EDC, highlighted by the Hutti (2547 ± 10 Ma), Kolar (2546 ± 12 Ma), and Jonnagiri (∼2545 Ma) deposits. Conversely, mineralization in the WDC and related structures occurred later, with hydrothermal xenotime dating establishing ages of 2522 ± 6 Ma at Gadag, 2520 ± 9 Ma at Ajjanahalli, and 2510 ± 12 Ma at Paramanahalli [106, 107].

The pressure–temperature–composition (*P*–*T*–*X*) characteristics of ore-forming fluids provide fundamental constraints on the genesis and evolution of gold mineralization in the Dharwar Craton [59]. The estimated pressure and temperature conditions of mineralization indicate formation over a relatively broad crustal interval but remain consistent with typical mesozonal orogenic gold systems. Most deposits record trapping pressures between approximately 1 and 4 kbar and temperatures of 240–400 °C, while some early mineralizing stages at Hutti and Uti reached temperatures exceeding 450 °C [23]. In the Western Dharwar Craton, deposits such as Gadag, Ajjanahalli, and Paramanahalli typically formed at ∼0.8–2.2 kbar and 260–330 °C, whereas deposits in the Eastern Dharwar Craton, including Hutti, Chigargunta, and Bisanatham, preserve evidence for mineralization at 1.5–3.5 kbar and up to ∼400 °C. These conditions correspond broadly to greenschist- to lower amphibolite-facies metamorphic environments and are compatible with fluid generation during regional metamorphic devolatilization. Hence, within the Dharwar Craton, in general, gold mineralization spans a wide range of *P*–*T* conditions (1–5 kbar; 220–450 °C) at the retrograde path from the peak amphibolite facies metamorphism.

The compositional (*X*) characteristics of the auriferous ore fluids further support a reduced, near-neutral hydrothermal system dominated by CO_2-rich aqueous solutions capable of transporting gold as bisulfide complexes, principally $Au(HS)_2^-$. Fluid inclusion studies indicate that phase separation or immiscibility, triggered by pressure fluctuations during fault-valve activity and episodic brittle–ductile deformation, was a major mechanism for destabilizing these complexes and precipitating gold. Additional processes such as fluid–rock interaction, sulfidation of Fe-bearing host rocks, and localized mixing with externally derived fluids further enhanced gold deposition. Although most deposits are characterized by CO_2-rich fluids, exceptions such as the Uti deposit contain relatively CO_2-poor aqueous fluids, suggesting local variations in fluid evolution and possible interaction with nearby granitoids.

Fluid inclusion investigations across major gold camps, including Hutti, Kolar, Chigargunta, Bisanatham, Jonnagiri, Gadag, Ajjanahalli, and Paramanahalli, demonstrate that the mineralizing fluids were predominantly low- to moderately saline aqueous–carbonic systems composed of H_2O–CO_2–NaCl with variable amounts of CH_4 and locally N_2. Salinities generally range from 1 to 13 wt% NaCl equivalent, although localized higher salinities have been reported where limited interaction with granitic fluids occurred.

Overall, the *P*–*T*–*X* characteristics of ore-forming fluids throughout the Dharwar Craton show remarkable consistency with globally recognized Archean orogenic gold systems. Their low salinity, aqueous–carbonic composition, moderate pressure–temperature conditions, and evidence for pressure-induced phase separation collectively support a predominantly metamorphic fluid source that migrated through crustal-scale shear zones and precipitated gold during late Neoarchean tectono-metamorphic events with except a few record of magmatic/juvenile fluid signature e.g. Hutti, Uti [59].

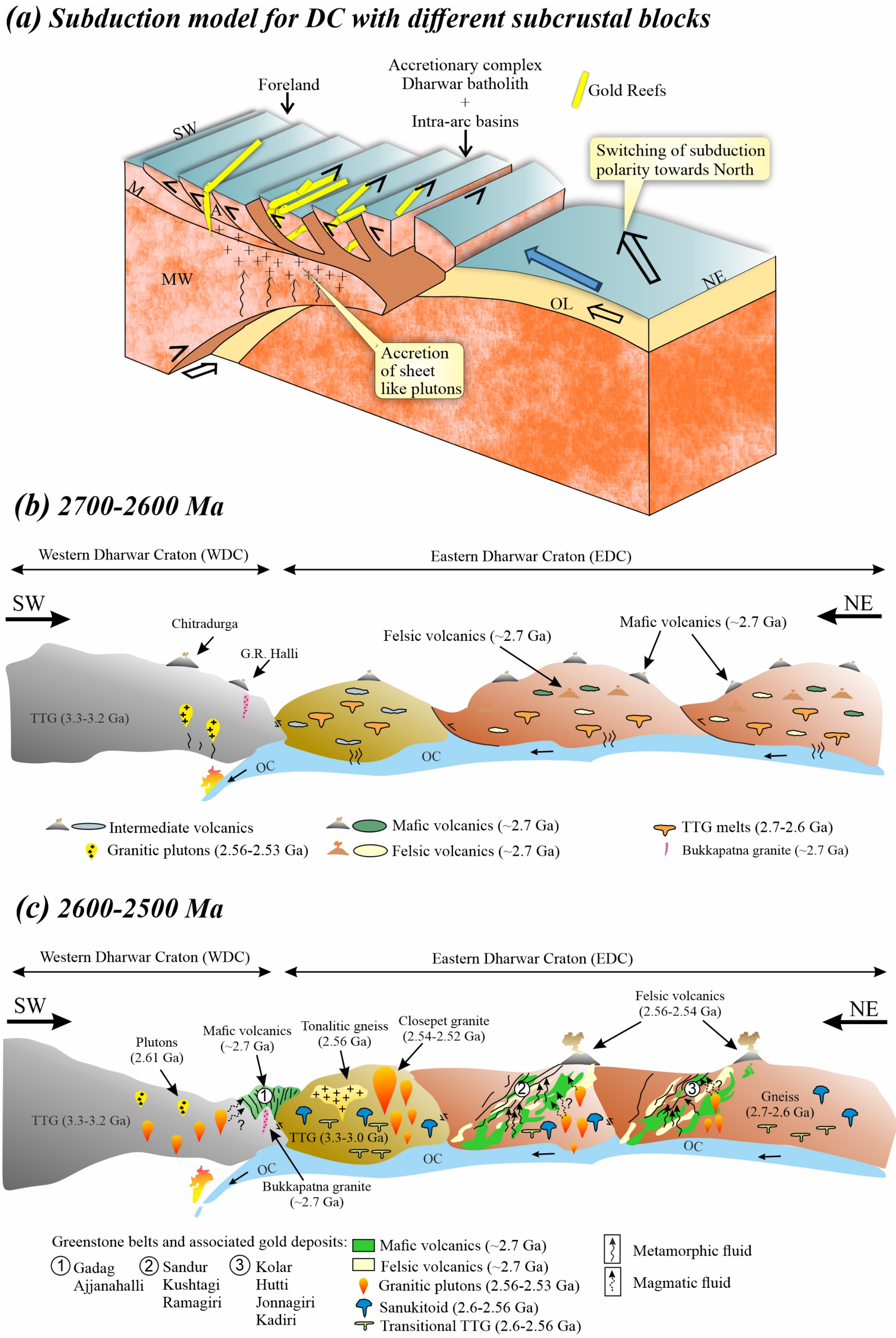

Figure 5. Schematic sketch illustrating generalized tectonic model for evolution of Dharwar craton and associated well known orogenic gold hosted greenstone belts (modified after [11, 103, 105]. See text for detailes).

Globally, orogenic gold deposits are characterized by relatively uniform low-salinity H_2O–NaCl–CO_2 ± CH_4 fluids [108]. According to [109], it is reported typical compositions of X_{CO_2} = 0.10–0.25, salinities of 3–7 wt% NaCl eq., and near-neutral pH, conditions widely compatible with metamorphic devolatilization. Although such fluids can also be generated by deep-seated granitic magmas (≥3 kbar; [110]) or Li–Be–rich pegmatitic systems [111], the geochronological relationships between granites and gold deposits are rarely consistent. Examples include mineralization that is older, younger, or synchronous with magmatism in the North American Cordillera [112], gold-hosting granites older than ores in the Yilgarn Craton [5], granites emplaced 60 Ma after mineralization in the Victorian Lachlan Fold Belt [113], and an absence of granitoids in the Otago Schist Belt. These discrepancies, coupled with the compositional uniformity of ore fluids, led [59] to conclude that a granitic-hydrothermal model is not universally applicable. Granitic-derived mantle fluids have also been proposed for select deposits for instance, carbon–oxygen isotope data from the Jonnagiri granitoid-hosted system [114]. However, the temporal mismatch between gold deposition, mantle metasomatism, and magma extraction weakens this interpretation. In the Murchison domain of the Yilgarn Craton, for example, sanukitoids (∼2.75 Ga) predate gold mineralization (∼2.65 Ga) by at least 100 Ma [115], contradicting the short-duration nature of orogenic systems. Conversely, the metamorphic model is strongly supported by global analogues.

4.3. Genesis of Gold Deposits in Dharwar Craton

Fluid release during greenschist–amphibolite transition metamorphism can efficiently mobilize Au, As, Hg, and Sb, as demonstrated in the actively deforming Southern Alps [116]. Major granitoid-hosted Archean gold deposits in the Yilgarn (Wallaby, Tarmoola, Granny Smith, Federal/Golden Cities), the Abitibi belt (Sigma–Lamaque, Renabie), and the only granitoid-hosted system in the Dharwar Craton (Jonnagiri) uniformly contain low-salinity H_2O–CO_2 ± CH_4 fluids of metamorphic origin. Metamorphic devolatilization at greenschist–amphibolite transitions releases large fluid volumes along crustal-scale shear zones [117], and thermodynamic models identify $Au(HS)_2^-$ as the dominant gold-transport complex under such H_2S-rich conditions [118, 119]. In both EDC and WDC, mineralization is broadly associated with uniform aqueous–carbonic fluids, except at Uti and in sulfide-rich lodes of Kolar (Oriental and McTaggart), where CO_2 is absent or minor. These patterns indicate that auriferous fluids were sourced predominantly from deep-crustal metamorphic devolatilization of the greenstone sequences, locally modified by higher-salinity granitic/juvenile inputs (e.g., Kolar, Hira-Buddini) supports a mixed fluid-source model. Migration of these fluids along crustal-scale shear systems, followed by fluid–rock interaction, fluid phase separation, and sulfidation within higher-order splays, facilitated gold precipitation throughout the Craton. The relatively younger age of gold mineralization in the Dharwar Craton reflects its prolonged Neoarchean tectono-magmatic evolution. Unlike many cratons that stabilized earlier, the Dharwar Craton continued to experience crustal thickening, deformation, and granitoid magmatism until ∼2.56–2.50 Ga. This late-stage geodynamic activity reactivated the Chitradurga, Kadiri, and Hutti shear systems, enabling the ascent of metamorphogenic auriferous fluids. These younger fluid pulses, intimately linked to last Neoarchean convergence and cratonization, produced gold deposits that are systematically younger than those in many globally recognized Archean orogenic provinces.

5. Conclusions

The following conclusion has been made based on the current review work:

- The Dharwar Craton hosts one of the world's most significant Neoarchean orogenic gold provinces, with gold mineralization spatially associated with greenstone belts, major crustal-scale shear zones, and syn- to late-tectonic granitoids.
- Gold mineralization is structurally controlled and predominantly localized within higher-order splays of regional shear systems, where focused fluid flow, deformation, and fluid–rock interaction created favourable sites for ore deposition.
- Peak metamorphic conditions across the gold camps range from greenschist- to amphibolite-facies, indicating that regional tectono-metamorphic evolution played a fundamental role in fluid generation and mineralization.
- Hydrothermal alteration is characterized by systematic assemblages dominated by carbonatization, sericitization, chloritization, silicification, sulfidation, and locally tourmalinization, providing reliable vectors toward mineralized zones.
- Geochronological data indicate that major gold mineralization occurred between approximately 2547 and 2510 Ma, broadly overlapping with regional metamorphism, juvenile granitoid emplacement, and late Neoarchean tectono-thermal events.
- Fluid inclusion studies reveal remarkably uniform low- to moderately saline H_2O–CO_2–NaCl ± CH_4 ore fluids formed at moderate temperatures and pressures, consistent with the physicochemical characteristics of Archean orogenic gold systems worldwide.
- Gold precipitation was principally driven by pressure fluctuations, fluid immiscibility, sulfidation of reactive host rocks, and fluid–rock interaction within dynamically reactivated shear zones, with local contributions from fluid mixing.
- Stable isotope systematics (O, H, C, S, and Sr), together with fluid inclusion and mineral chemistry

data, indicate that the ore fluids were dominated by metamorphic components but were locally modified by magmatic inputs and crustal interactions.

- The temporal overlap of bimodal volcanism, greenstone metamorphism, juvenile granitoid magmatism, and gold mineralization, combined with craton-wide similarities in ore-fluid composition and isotopic signatures, supports a mixed fluid-source model in which metamorphic fluids constitute the dominant component while magmatism provides heat and localized volatile contributions.
- Accessory mineral geochemistry, particularly of tourmaline, pyrite, and arsenopyrite, records evolving hydrothermal conditions and episodic fluid influx, offering valuable insights into ore-forming processes and exploration targeting.
- The synthesis of geological, structural, geochronological, fluid inclusion, stable isotope, and mineral chemical datasets demonstrates that the Dharwar Craton represents an integrated orogenic gold system generated during late Neoarchean crustal reworking and fluid focusing along long-lived transcrustal structures.
- Future research integrating high-resolution geochronology, *in situ* isotopic analyses, and trace-element mapping of ore-related minerals will be essential to further resolve the relative contributions of metamorphic and magmatic fluids and to refine predictive exploration models for concealed gold deposits in the Dharwar Craton.

Author Contributions

S.S.C.: Conceptualization, Visualization, Funding acquisition, Investigation, Formal analysis, Supervision Writing—original draft. D.P.: Data curation, Writing—review & editing. M.J.S.: Data curation Writing—original draft review and editing. M.S.: Data curation, Writing—review and editing.

Funding

DST-SERB, Government of India: Deep Continental Studies (ESS/16/259/2005), Young Scientist Scheme (YSS/2015/000960); Core Research Grants (EMR/2017/003216) (SERB-CRG/2021/004129); IRCC-IIT Bombay: Seed Grant (RD/0519-IRCCSH0-005).

Institutional Review Board Statement

Not applicable.

Informed Consent Statement

Not applicable.

Data Availability Statement

All data used in this work are presented in the paper.

Acknowledgements

This review article compiles the work of the S.S.C. and his collaborators and students over the past two decades and integrates other published literature available in the public domain. The author thanks all the master's students who contributed to data generation on these deposits. The author acknowledges the support of collaborative industry partners, including the Geological Survey of India (GSI), Ramgad Minerals & Mining Limited (RMML) Baldota, and Geomysore India Private Ltd. The first author also thanks the funding agencies: DST-SERB, Government of India; IRCC-IIT Bombay through the Young Scientist Scheme (YSS/2015/000960); the Core Research Grant (EMR/2017/003216); and the Seed Grant (RD/0519-IRCCSH0-005) respectively awarded to SSC and his collaborator, Biswajit Mishra (ESS/16/259/2005). Krishnamurthi (SERB-CRG/2021/004129). We sincerely thank M.L. Dora and an anonymous journal reviewer for their insightful comments and Abhisikta Goswami and Cheng-Xue Yang, for their timely editorial handling and helpful suggestions. Finally, S.S.C. thanks M. Santosh for the invitation to write this review on orogenic gold deposits in the Dharwar craton.

Conflicts of Interest

The authors declare that they have no known competing financial interests or personal relationships that could have appeared to influence the work reported in this paper

Use of AI and AI-assisted Technologies

No AI assisted tools were used during the preparation of this paper except for correcting the style of English and grammar. The authors carefully reviewed the manuscript and takes full responsibility of the content.

References

1. Tomkins, A.G. On the source of orogenic gold. *Geology* **2013**, *41*, 1255–1256. https://doi.org/10.1130/focus122013.1
2. Frimmel, H.E.; Hennigh, Q. First whiffs of atmospheric oxygen triggered onset of crustal gold cycle. *Miner. Depos.* **2015**, *50*, 5–23. https://doi.org/10.1007/s00126-014-0574-8
3. Böhlke, J.K. Orogenic (metamorphic-hosted) gold-quartz veins. *U.S. Geol. Surv. Open-File Rep.* **1982**, *795*, 70–76.
4. Groves, D.I. The crustal continuum model for late Archean lode gold deposits of the Yilgarn Block, Western Australia. *Miner. Depos.* **1993**, *28*, 366–374. https://doi.org/10.1007/BF02431596
5. Goldfarb, R.J.; Groves, D.I. Orogenic gold: Common or evolving fluid and metal sources through time. *Lithos* **2015**, *233*, 2–26. https://doi.org/10.1016/j.lithos.2015.07.011
6. Phillips, G.N.; Powell, R. Formation of gold deposits: Review and evaluation of the continuum model. *Earth-Sci. Rev.* **2009**, *94*, 1–21. https://doi.org/10.1016/j.earscirev.2009.02.002
7. Phillips, G.N.; Powell, R. Formation of gold deposits: A metamorphic devolatilization model. *J. Metam. Geol.* **2010**, *28*, 689–718. https://doi.org/10.1111/j.1525-1314.2010.00887.x
8. Tomkins, A.G.; Grundy, C. Upper temperature limits of orogenic gold deposit formation: Constraints from the granulite-hosted Griffin's Find deposit, Yilgarn Craton. *Econ. Geol.* **2009**, *104*, 669–685. https://doi.org/10.2113/gsecongeo.104.5.669

9. Tomkins, A.G. Windows of metamorphic sulphur liberation in the crust: Implications for gold deposit genesis. *Geochim. Cosmochim. Acta* **2010**, *74*, 3246–3259. https://doi.org/10.1016/j.gca.2010.03.003

10. Gaboury, D. Parameters for the formation of orogenic gold deposits. *Appl. Earth Sci.* **2019**, *128*, 124–133. https://doi.org/10.1080/25726838.2019.1583310

11. Jayananda, M.; Peucat, J.J.; Chardon, D.; Krishna Rao, B.; Fanning, C.M. Neoarchean 788 greenstone volcanism and continental growth, Dharwar Craton, southern India: 789 Constraints from SIMS U–Pb zircon geochronology and Nd isotopes. Precambrian 790 *Res.* **2013**, *227*, 55–76.

12. Mishra, B.; Pal, N.; Basu Sarbadhikari, A. Fluid inclusion characteristics in barren and auriferous quartz veins in the Uti gold deposit, Hutti-Maski greenstone belt, southern India. *Ore Geol. Rev.* **2005**, *16*, 1–16. https://doi.org/10.1016/j.oregeorev.2004.10.002

13. Kolb, J.; Rogers, A.; Meyer, F.M. Relative timing of deformation and two-stage gold mineralization at Hutti Mine, Dharwar Craton, India. *Miner. Depos.* **2004**, *40*, 156–174. https://doi.org/10.1007/s00126-005-0475-y

14. Ramakrishnan, M.; Vaidyanadhan, R. Cratons. In *Geology of India*; Geological Society of India: Bangalore, India, 2008; Volume 1, pp. 99–180.

15. Rogers, A.J.; Kolb, J.; Meyer, F.M.; et al. Two stages of gold mineralization at Hutti Mine, India. *Miner. Depos.* **2013**, *48*, 99–114. https://doi.org/10.1007/s00126-012-0416-5

16. Rogers, A.J.; Kolb, J.; Meyer, F.M.; et al. Tectono-magmatic evolution of the Hutti-Maski greenstone belt, India: Constrained using geochemical and geochronological data. *J. Asian Earth Sci.* **2007**, *31*, 55–70. https://doi.org/10.1016/j.jseaes.2007.04.003

17. Manikyamba, C.; Kerrich, R.; Khanna, T.C.; et al. Enriched and depleted arc basalts, with Mg-andesites and adakites: A potential paired arc-back arc of the 2.6 Ga Hutti greenstone terrane, India. *Geochim. Cosmochim. Acta* **2009**, *73*, 1711–1736. https://doi.org/10.1016/j.gca.2008.12.020

18. Kolb, J.; Rogers, A.; Meyer, F.M.; et al. Development of fluid conduits in the auriferous shear zones of the Hutti Gold Mine, India: Evidence for spatially and temporally heterogeneous fluid flow. *Tectonophysics* **2004**, *378*, 65–84. https://doi.org/10.1016/j.tecto.2003.10.009

19. Roy, A. Polyphase folding deformation in the Hutti-Maski schist belt, Karnataka. *J. Geol. Soc. India* **1979**, *20*, 598–607.

20. Roy, A. The geology of gold mineralization at Hutti in Hutti-Maski schist belt, Karnataka, India. *Indian Miner.* **1991**, *45*, 229–250.

21. Sangurmath, P. Uti gold deposit—evolving scene, Hutti-Maski greenstone belt, Karnataka, India. *Geol. Surv. India Spec. Publ.* **2001**, *58*, 289–292.

22. Curtis, L.C.; Radhakrishna, B.P. *Hutti Gold Mine into the 21st Century*; Geological Society of India: Bangalore, India, 1995; p. 176.

23. Mishra, B.; Pal, N. Metamorphism, fluid flux, and fluid evolution relative to gold mineralization in the Hutti-Maski greenstone belt, Eastern Dharwar Craton, India. *Econ. Geol.* **2008**, *103*, 801–827. https://doi.org/10.2113/gsecongeo.103.4.801

24. Robert, F.; Poulsen, K.H. Vein formation and deformation in greenstone gold deposits. *Rev. Econ. Geol.* **2001**, *14*, 111–155. https://doi.org/10.5382/Rev.14.05

25. Narayanswami, S.; Ziauddin, M.; Ramachandra Rao, A. Structural control and localization of gold-bearing lode, Kolar Gold Field, India. *Econ. Geol.* **1960**, *55*, 1429–1459.

26. Hamilton, J.V.; Hodgson, C.J. Mineralization and structure of the Kolar Gold Field, India. In *Gold '86*; MacDonald, A.J., Ed.; Konsult Int. Inc.: Willowdale, ON, Canada, 1986; pp. 270–283.

27. Mukhopadhyay, D.K. Significance of small-scale structures in the Kolar schist belt, South India. *J. Geol. Soc. India* **1989**, *33*, 291–308.

28. Sheshadri, C.R. Indian gold production. *Min. Ann. Rev. Min. Mag.* **1988**, 435–445.

29. Radhakrishna, B.P.; Curtis L.C. *Gold: The Indian scene*; Geological Society of India: Bangalore, India, 1991; p. 163.

30. Radhakrishna, B.P.; Curtis, L.C. Gold in India. *J. Geol. Soc. India* **1999**, *53*, 308.

31. Pal, D. Genesis of Gold Mineralization in the South Kolar and Gadag Greenstone Belts, Dharwar Craton: Constraints from Hydrothermal Alteration, Tourmaline Chemistry, Fluid Inclusion and Stable Isotope Studies. Ph.D. Thesis, NIT Rourkela, Rourkela, Odisha, India, 2022.

32. Pal, D.; Chinnasamy, S.S.; Goon, S.; et al. Alteration mineralogy, fluid inclusions and stable isotope studies from Chigargunta and Bisanatham gold deposits, South Kolar Greenstone Belt, Dharwar Craton, India: Implications on genesis of gold mineralization. *Ore Geol. Rev.* **2019**, *111*, 102946. https://doi.org/10.1016/j.oregeorev.2019.102946

33. Pal, D.; Chinnasamy, S.S.; Goon, S. Characterization of hydrothermal alteration at Chigargunta and Bisanatham gold deposits, South Kolar Greenstone Belt, Dharwar Craton, India. *J. Geol. Soc. India, Spec. Publ.* **2021**, *11*, 40–45.

34. Jairam, M.S.; Roop Kumar, D.; Srinivasan, K.N. Classification of greenstone and associated granitoids of Jonnagiri schist belt, Kurnool district, Andhra Pradesh. *Geol. Surv. India Spec. Publ.* **2001**, *55*, 59–66.

35. Saravanan, C.S.; Mishra, B.; Jairam, M.S. P–T conditions of mineralization in the Jonnagiri granitoid-hosted gold deposit, Eastern Dharwar Craton, southern India: Constraints from fluid inclusions and chlorite thermometry. *Ore Geol. Rev.* **2009**, *36*, 333–349. https://doi.org/10.1016/j.oregeorev.2009.07.004

36. Chinnasamy, S.S.; Mishra, B. Greenstone metamorphism, hydrothermal alteration, and gold mineralization in the genetic context of the granodiorite-hosted gold deposit at Jonnagiri, Eastern Dharwar Craton, India. *Econ. Geol.* **2013**, *108*, 1015–1036. https://doi.org/10.1016/j.oregeorev.2009.07.004

37. Rao, K.S.; Kumar, D.R.; Jairam, M.S.; et al. Interpretation of geological characteristics of Dona gold prospect, Jonnagiri schist belt, Kurnool district, Andhra Pradesh. *Geol. Surv. India Spec. Publ.* **2001**, *58*, 217–231.

38. Vasudev, V.N. *Field Guide to Selected Gold Prospects in Karnataka and Andhra Pradesh*; Geological Society of India: Bangalore, India, 2009.

39. Bhattacharya, S.; Panigrahi, M.K.; Sachan, H.K.; et al. Oxygen isotope ratio of quartz veins from the auriferous Ramagiri-Penakacherla schist belt and surrounding granitoids in the Eastern Dharwar Craton: A case for possible link between gold mineralization and granite magmatism. *Ore Geol. Rev.* **2014**, *63*, 201–208. https://doi.org/10.1016/j.oregeorev.2014.04.023

40. Ugarkar, A.G.; Malapur, M.A.; Kumar, B.C. Archean turbidite-hosted orogenic gold mineralization in the Gadag greenstone belt, Western Dharwar Craton, Peninsular India. *Ore Geol. Rev.* **2016**, *72*, 1224–1242. https://doi.org/10.1016/j.oregeorev.2014.04.023

41. Chadwick, B.; Vasudev, V.N.; Hegde, G.V. The Chitradurga schist belt and its adjacent plutonic rocks, NW of Tungabhadra, Karnataka: A duplex in the Late Archaean convergent setting of the Dharwar Craton. *J. Geol. Soc. India* **2003**, *61*, 645–663.

42. Pal, D.; Saikia M.J.; Chinnasamy, S.S.; et al. Fluid inclusion, stable isotope and tourmaline chemistry at Gadag Gold Field, Dharwar Craton, India: Implications for metamorphic origin of auriferous fluid, *Ore Geol. Rev.* **2025**, *186*, 106876. https://doi.org/10.1016/j.oregeorev.2025.106876

43. Mukhopadhyay, D.; Baral, M.C. Structural geometry of Dharwar rocks near Chitradurga in the Chitradurga schist belt. *J. Geol. Soc. India* **1985**, *26*, 547–566.

44. Pal, N.; Mishra, B. Epigenetic nature of BIF-hosted gold mineralization at Ajjanahalli, southern India: Evidence from ore petrography and fluid inclusion studies. *Gondwana Res.* **2003**, *6*, 531–540.

https://doi.org/10.1016/S1342-937X(05)70836-2

45. Dharuman, R. *Final Report on the Preliminary Exploration for Gold in Paramanahalli Block, Chitradurga Schist Belt, Chitradurga District, Karnataka (Part A and B)*; Geological Survey of India Report; Geological Survey of India (GSI): Kolkata, India, 2004.
46. Sati, M.; Krishnamurthi, R.; Chinnasamy, S.S.; et al. Gold mineralization at Paramanahalli prospect, Chitradurga Greenstone Belt, Western Dharwar Craton, Karnataka, India. *J. Geol. Soc. India* **2025**, *101*, 397–405. https://doi.org/10.17491/jgsi/2025/174104
47. Sati, M.; Krishnamurthi, R.; Saravanan, S.; et al. Mineralogy, hydrothermal alteration and paragenesis of gold mineralization at Paramanahalli prospect, Chitradurga Greenstone Belt. *Ore Geol. Rev.* **2025**, *176*, 106398. https://doi.org/10.1016/j.oregeorev.2024.106398
48. Gopalakrishna, G.; Shareef, M.; Nagesh, P.C. Shear-controlled gold mineralization of GR Halli area of Chitradurga Schist Belt, Dharwar Craton: Insights from fluid inclusion study. *Open J. Geol.* **2018**, *8*, 662–673. https://doi.org/10.4236/ojg.2018.88041
49. Khan, S.A. Gold mineralization along Gonur-Jagalur shear corridor in the central part of the Chitradurga schist belt, Karnataka. In *National Seminar on Exploration and Survey for Noble Metals and Precious Stones*; Geol. Surv. India Spec. Publ. 58; Geological Survey of India (GSI): Kolkata, India, 2001; pp.251–261.
50. Gupta, S.; Jayananda, M. Tourmaline from Archean G.R. Halli gold deposit, Chitradurga greenstone belt, Dharwar Craton (India): Implications for the gold metallogeny. *Geosci. Front.* **2014**, *5*, 877–892. https://doi.org/10.1016/j.gsf.2013.12.002
51. Pandalai, H.S.; Jadhav, G.N.; Mathew, B.; et al. Dissolution channels in quartz and the role of pressure changes in gold and sulfide deposition in the Archean greenstone-hosted Hutti gold deposit, Karnataka, India: Petrography and fluid inclusion studies. *Miner. Depos.* **2003**, *38*, 597–624. https://doi.org/10.1007/s00126-003-0357-1
52. Badhe, K.V; Pandalai, H.S.; Pande, K. 40Ar-39Ar age constraints on timing of a late hydrothermal event in the Hutti greenstone belt, Karnataka, India. *J. Asian Earth Sci.* **2019**, *172*, 115–125. https://doi.org/10.1016/j.jseaes.2018.12.026
53. Hazarika, P.; Pruseth, K.L.; Mishra, B. Neoarchean greenstone metamorphism in the Eastern Dharwar Craton, India: Constraints from monazite U–Th–Pb total ages and P–T pseudosection calculations. *J. Geol.* **2015**, *123*, 429–461. https://doi.org/10.1086/681719
54. Rajamani V; Shivkumar K; Hanson G.N.; Granath J.W. Petrogenesis of Amphibolites in the Kolar Schist Belt, India-A Preliminary Report. *Jour. Geol. Soc. India* **1981**, *22 911*, 470–487.
55. Sarma, D.S.; McNaughton, N.J.; Fletcher, I.R.; et al. Timing of gold mineralization in the Hutti gold deposit, Dharwar Craton, South India. *Econ. Geol.* **2008**, *103*, 1715–1727. https://doi.org/10.2113/gsecongeo.103.8.1715
56. Sarangi, S.; Sarkar, A.; Srinivasan, S.; et al. Carbon isotope studies of auriferous quartz-carbonate veins from two orogenic gold deposits from the Neoarchean Chitradurga schist belt, Dharwar Craton, India: Evidence for mantle/magmatic source of auriferous fluid. *J. Asian Earth Sci.* **2012**, *52*, 1–11. https://doi.org/10.1016/j.jseaes.2011.12.004
57. Kolb, J.; Hellmann, A.; Rogers, A.; et al. The role of a transcrustal shear zone in orogenic gold mineralization at the Ajjanahalli Mine, Dharwar Craton, South India. *Econ. Geol.* **2004**, *99*, 743–759. https://doi.org/10.2113/gsecongeo.99.4.743
58. Saikia, M.J. Genesis of Gold Mineralization in the Gadag Greenstone Belt, Western Dharwar Craton: Insights from Greenstone Metamorphism, Alteration Geochemistry and Ore Mineralogy. Ph.D. Thesis, Indian Institute of Technology Bombay, Mumbai, India, 2025.
59. Mishra, B.; Pruseth, K.L.; Hazarika, P.; et al. Nature and source of the ore-forming fluids associated with orogenic gold deposits in the Dharwar Craton. *Geosci. Front.* **2018**, *9*, 715–726. https://doi.org/10.1016/j.gsf.2017.09.005
60. Sahoo, A.K.; Krishnamurthi, R.; Sangurmath, P. Nature of ore-forming fluids, wall rock alteration and P–T conditions of gold mineralization at Hira-Buddini, Hutti-Maski Greenstone Belt, Dharwar Craton, India. *Ore Geol. Rev.* **2018**, *99*, 195–216. https://doi.org/10.1016/j.oregeorev.2018.06.008
61. Santosh, M. Ore fluids in the auriferous Champion Reef of Kolar, South India. *Econ. Geol.* **1986**, *81*, 1546–1552. https://doi.org/10.2113/gsecongeo.81.6.1546
62. Gupta, S.; Fareeduddin. Occurrence of paragonite in the hydrothermal wall rock alteration zone of G.R. Halli gold deposit, Chitradurga Schist Belt, Western Dharwar Craton, southern India. *J. Geol. Soc. India* **2013**, *82*, 461–473.
63. Sarma, D.S.; Fletcher, I.R.; Rasmussen, B.; et al. Archaean gold mineralization synchronous with late cratonization of the Western Dharwar Craton, India: Evidence from SHRIMP U–Pb geochronology of xenotime in gold deposits. *Miner. Depos.* **2011**, *46*, 273–288. https://doi.org/10.1007/s00126-010-0326-3
64. Deb, M. Precambrian geodynamics and metallogeny of the Indian Shield. *Ore Geol. Rev.* **2014**, *57*, 1–28. https://doi.org/10.1016/j.oregeorev.2013.08.022
65. Anand, R.; Balakrishnan, S. Pb, Sr and Nd isotope systematics of metavolcanic rocks of the Hutti greenstone belt, Eastern Dharwar Craton: Constraints on age, duration of volcanism and evolution of mantle sources during the Late Archean. *J. Asian Earth Sci.* **2010**, *39*, 1–11. https://doi.org/10.1016/j.jseaes.2010.02.010
66. Anand, R.; Balakrishnan, S.; Mezger, K. Geochemical and geochronological studies on titanites from the granitoid rocks of the Eastern Dharwar Craton, South India. *Geophys. Res. Abstr.* **2005**, *7*, 1607-7962/gra/EGU1605-A-01565.
67. Vasudev, V.N.; Chadwick, B.; Nutman, A.P.; et al. Rapid development of the Late Archean Hutti schist belt, northern Karnataka: Implications of new field data and SHRIMP U/Pb zircon ages. *J. Geol. Soc. India* **2000**, *55*, 529–540.
68. Balakrishnan, S.; Rajamani, V.; Hanson, G.N. U–Pb ages for zircon and titanite from the Ramagiri area, southern India: Evidence for the accretionary origin of the Eastern Dharwar Craton during the Late Archean. *J. Geol.* **1999**, *107*, 69–86. https://doi.org/10.1086/314331
69. Krogstad, E.J.; Hanson, G.N.; Rajamani, V. U–Pb ages of zircon and sphene for two gneiss terranes adjacent to the Kolar schist belt, South India: Evidence for separate crustal evolution histories. *J. Geol.* **1991**, *99*, 421–434. https://doi.org/10.1086/629553
70. Balakrishnan, S.; Hanson, G.N.; Rajamani, V. Pb and Nd isotope constraints on the origin of high-Mg and tholeiitic amphibolites, Kolar schist belt, South India. *Contrib. Mineral. Petrol.* **1990**, *107*, 279–292. https://doi.org/10.1007/BF00325099
71. Das, S.; Chinnasamy, S.S. Granitoids of the Jonnagiri greenstone belt of eastern Dharwar craton: Constraints from geochemistry and U-Pb zircon geochronology [Conference presentation]. In *EGU General Assembly 2024*; European Geosciences Union (EGU) / Copernicus Publications (EGUsphere platform): Vienna, Austria, 2024. https://doi.org/10.5194/egusphere-egu24-6082
72. Ram Mohan, M.; Sarma, D.S.; Neal, J.M.; et al. SHRIMP zircon and titanite U–Pb ages, Lu–Hf isotope signatures and geochemical constraints for ∼2.56 Ga granitic magma in the Western Dharwar Craton, southern India: Evidence for short-lived Neoarchean episodic crustal growth? *Precambrian Res.* **2014**, *243*, 197–220. https://doi.org/10.1016/j.precamres.2013.12.017
73. Sarma, D.S.; McNaughton, N.J.; Belousova, E.; et al. Detrital zircon U–Pb ages and Hf-isotope systematics from the Gadag greenstone belt: Archean crustal growth in the Western Dharwar Craton, India. *Gondwana Res.* **2012**, *22*, 843–854. https://doi.org/10.1016/j.gr.2012.04.001
74. Sati, M.; Krishnamurthi, R.; Saravanan, S. Monazite chemistry and timing of mineralization at Paramanahalli, Chitradurga Greenstone Belt, Dharwar Craton, India: Implications

for gold exploration. *J. Geochem. Explor.* **2025**, *271*, 107688. https://doi.org/10.1016/j.gexplo.2025.107688

75. Pal, N.; Mishra, B. Alteration geochemistry and fluid inclusion characteristics of the greenstone-hosted gold deposit at Hutti, Eastern Dharwar Craton, India. *Miner. Depos.* **2002**, *37*, 722–736. https://doi.org/10.1007/s00126-002-0257-8
76. Hazarika, P.; Mishra, B.; Pruseth, K.L. Scheelite, apatite, calcite and tourmaline compositions from the Late Archean Hutti orogenic gold deposit: Implications for analogous two-stage ore fluids. *Ore Geol. Rev.* **2016**, *72*, 989–1003. https://doi.org/10.1016/j.oregeorev.2015.09.004
77. Krienitz, M.S.; Trumbull, R.B.; Hellmann, A.; et al. Hydrothermal gold mineralisation at the Hira-Buddini gold mine, India: Constraints on fluid evolution and fluid sources from boron isotopic compositions of tourmaline. *Miner. Depos.* **2008**, *43*, 421–434. https://doi.org/10.1007/s00126-007-0172-0
78. Saravanan, C.S.; Mishra, B. Uniformity in sulphur isotope compositions in the orogenic gold deposit from the Dharwar Craton, southern India. *Miner. Depos.* **2009**, *44*, 597–605. https://doi.org/10.1007/s00126-009-0241-7
79. Sinha, M. Gold Mineralization in the Western Ramagiri Block, Anantapur District, Andhra Pradesh, with Special Reference to Fluid Inclusion Characteristics. Master's Thesis, Indian Institute of Technology Kharagpur, Kharagpur, India, 1997, *unpublished*.
80. Hazarika, P.; Mishra, B.; Pruseth, K.L. Diverse tourmaline compositions from orogenic gold deposits in the Hutti-Maski greenstone belt, India: Implications for sources of ore-forming fluids. *Econ. Geol.* **2015**, *110*, 337–353. https://doi.org/10.2113/econgeo.110.2.337
81. Giritharan, T.S., Rajamani, V. REE geochemistry of ore zones in the archean auriferous schist belts of the eastern Dharwar Craton, south India. *J. Earth Syst. Sci.* **2001**, *110*, 143–159. https://doi.org/10.1007/BF02702214
82. Bhattacharya, S.; Panigrahi, M.K. Heterogeneity in fluid characteristics in the Ramagiri–Penakacherla sector of the Eastern Dharwar Craton: Implications to gold metallogeny. *Russ. Geol. Geophys.* **2011**, *52*, 1436–1447. https://doi.org/10.1016/j.rgg.2011.10.012
83. Mishra, B.; Panigrahi, M.K. Fluid evolution in Kolar Gold Field: Evidence from fluid inclusion studies. *Miner. Depos.* **1999**, *34*, 173–181. https://doi.org/10.1007/s001260050194
84. Swain, S.K.; Sarangi, S.; Srinivasan, R.; et al. Isotope (C and O) composition of auriferous quartz-carbonate veins, central lode system, Gadag Gold Field, Dharwar Craton, India: Implications to source of ore fluids. *Ore Geol. Rev.* **2015**, *70*, 305–320. https://doi.org/10.1016/j.oregeorev.2015.03.020
85. Malapur, M.A.; Manjunatha, S.; Chandan Kumar, B.; et al. Ore fluids associated with the metasediment-hosted Central Auriferous Zones of Gadag Gold Field, Karnataka. *Int. J. Earth Sci. Eng.* **2012**, *5*, 1545–1551.
86. Naden, J.; Shepherd, T.J. Role of methane and carbon dioxide in gold deposition. *Nature* **1989**, *342*, 793–795. https://doi.org/10.1038/342793a0
87. Wilkinson, J.J. Fluid inclusions in hydrothermal ore deposits. *Lithos* **2001**, *55*, 229–272. https://doi.org/10.1016/S0024-4937(00)00047-5
88. McCuaig, T.C.; Kerrich, R. P–T–t deformation fluid characteristics of lode gold deposits: Evidence from alteration systematics. *Ore Geol. Rev.* **1998**, *12*, 381–453. https://doi.org/10.1016/S0169-1368(98)80002-4
89. Sillitoe, R.H.; Thompson, J.F.H. Intrusion-related vein gold deposits: Types, tectono-magmatic settings and difficulties of distinction from orogenic gold deposits. *Res. Geol.* **1998**, *48*, 237–250. https://doi.org/10.1111/j.1751-3928.1998.tb00021.x
90. Thompson, J.F.H.; Sillitoe, R.H.; Baker, T.; et al. Intrusion-related gold deposits associated with tungsten-tin provinces. *Miner. Depos.* **1999**, *34*, 323–334. https://doi.org/10.1007/s001260050207
91. Groves, D.I.; Goldfarb, R.J.; Robert, F.; et al. Gold deposits in metamorphic belts: Overview of current understanding, outstanding problems, future research, and exploration significance. *Econ. Geol.* **2003**, *98*, 1–29. https://doi.org/10.2113/gsecongeo.98.1.1
92. Menon, A.G.; Venkatasubramanian, V.S.; Vasudev, V.N.; et al. Sulfur isotope abundance variations in sulfides of the Dharwar Craton—Part III: Hutti. *J. Geol. Soc. India* **1981**, *22*, 448–450.
93. Lambert, I.B.; Phillips, G.N.; Groves, D.I. Sulfur isotope compositions and genesis of Archean gold mineralisation, Australia and Zimbabwe. *Geol. Soc. Zimbabwe Spec. Publ.* **1984**, *1*, 373–387.
94. Selvaraja, V.; Caruso, S.; Fiorentini, M.L.; et al. Atmospheric sulfur in the orogenic gold deposits of the Archean Yilgarn Craton, Australia. *Geology* **2017**, *45*, 691–694. https://doi.org/10.1130/G39018.1
95. Shieh, Y.; Taylor, H.P. Oxygen and carbon isotope studies of contact metamorphism of carbonate rocks. *J. Petrol.* **1969**, *10*, 307–331. https://doi.org/10.1093/petrology/10.2.307
96. Ohmoto, H.; Goldhaber, M.B. Geochemistry of hydrothermal ore deposits. In *Geochemistry of Hydrothermal Ore Deposits*, 3rd ed.; John Wiley & Sons: New York, NY, USA, 1997; pp. 517–611.
97. Jiang, S.Y.; Yu, J.M.; Lu, J.J. Trace and rare-earth element geochemistry in tourmaline and cassiterite from the Yunlong tin deposit, Yunnan, China: Implications for magmatic-hydrothermal fluid evolution and ore genesis. *Chem. Geol.* **2004**, *209*, 193–213. https://doi.org/10.1016/j.chemgeo.2004.04.021
98. Slack, J.F.; Trumbull, R.B. Tourmaline as a recorder of ore-forming processes. *Elements* **2011**, *7*, 321–326. https://doi.org/10.2113/gselements.7.5.321
99. Cabral, A.R.; Wiedenbeck, M.; Koglin, N.; et al. Boron-isotopic constraints on the petrogenesis of hematitic phyllite in the southern Serra do Espinhaço, Minas Gerais, Brazil. *Lithos* **2012**, *140*, 224–233. https://doi.org/10.1016/j.lithos.2012.01.011
100. Craig, J.R.; Vokes, F.M.; Solberg, T.N. Pyrite: Physical and chemical textures. *Miner. Depos.* **1998**, *34*, 82–101. http://dx.doi.org/10.1007/s001260050187
101. Large, R.R.; Maslennikov, V.V.; Robert, F.; et al. Multistage sedimentary and metamorphic origin of pyrite and gold in the giant Sukhoi Log deposit, Lena gold province, Russia. *Econ. Geol.* **2007**, *102*, 1233–1267. https://doi.org/10.2113/gsecongeo.102.7.1233
102. Cook, N.J.; Ciobanu, C.I.; Meria, D.; et al. Arsenopyrite-pyrite association in an orogenic gold ore: Tracing mineralization history from textures and trace elements. *Econ. Geol.* **2013**, *108*, 1273–1283. https://doi.org/10.2113/econgeo.108.6.1273
103. Jayananda, M.; Santosh, M.; Aadhiseshan, K.R. Formation of Archean (3600–2500 Ma) continental crust in the Dharwar Craton, southern India. *Earth-Sci. Rev.* **2018**, *181*, 12–42. https://doi.org/10.1016/j.earscirev.2018.03.013
104. Chinnasamy, S.S. Orogenic gold deposits in the Dharwar Craton: Current insights and future prospects. *J. Geol. Soc. India* **2025** *101*, 1290–1292. https://doi.org/10.17491/jgsi/2025/174236
105. Vasudev, V.N; Chinnasamy, S.S. Orogenic gold deposits of the Archaean Dharwar Craton: Development of Neoarchaean greenstone belts in a Phanerozoic-style plate-tectonic framework: A synthesis. *J. Geol. Soc. India* **2026**, *102*, 891–904.
106. Hazarika, P.; Mishra, B.; Pruseth, K.L. Trace element geochemistry of pyrite and arsenopyrite: Ore genetic applications for Late Archean orogenic gold deposits in southern India. *Mineral. Mag.* **2017**, *81*, 661–678. https://doi.org/10.1180/minmag.2016.080.128
107. Chinnasamy, S.S.; Hazarika, P.; Pal, D.; et al. Pyrite textures and trace element compositions from the granodiorite-hosted gold deposit at Jonnagiri, Eastern Dharwar Craton, India: Implications for gold mineralization processes. *Econ. Geol.* **2021**, *116*, 559–579. https://doi.org/10.5382/econgeo.4787
108. Garofalo, P.S.; Fricker, M.B.; Günther, D.; et al. Physical-chemical properties and metal budget of Au gold-transporting hydrothermal fluids in orogenic deposits. Geological Society, London, Special

Publications: London, UK, 2014. https://api.semanticscholar.org/CorpusID:129619918.

109. Ridley, J.R.; Diamond, L.W. Fluid chemistry of orogenic lode gold deposits and implications for genetic models. In *Gold in 2000. Reviews in Economic Geology*; Hagemann S.G., Brown P. , Eds.; Society of Economic Geologists, Inc.: Littleton, CO, USA, 200; Volume 13, pp. 141–162.

110. Eggler, D.H.; Kadik, A.A. The system $NaAlSi_3O_8$-H_2O-CO_2 to 20 kbar pressure: Compositional and thermodynamic relations of liquids and vapors coexisting with albite. *Am. Mineral.* **1979**, *64*, 1036–1048.

111. Cameron, E.N.; Rowe, R.B.; Weis, P.L. Fluid inclusions in beryl and quartz from pegmatites of the Middletown district, Connecticut. *Am. Mineral.* **1953**, *38*, 218–262.

112. Goldfarb, R.J.; Hart, C.J.R.; Marsh, E.E. Orogenic gold and evolution of the Cordilleran orogen. In *Circum-Pacific Tectonics, Geologic Evolution and Ore Deposits*; Spencer, J.E., Titley, S.R., Eds.; Arizona Geological Society Digest 22; Arizona Geological Society: Tucson, AZ, USA, 2008; pp. 311–323.

113. Bierlein, F.P.; Arne, D.C.; Foster, D.A.; et al. A geochronological framework for orogenic gold mineralization in Central Victoria, Australia. *Miner. Depos.* **2001**, *36*, 741–767. https://doi.org/10.1007/s001260100203

114. Kesarwani, M.; Sarangi, S.; Srinivasan, R.; et al. Origin of granodiorite-hosted Neoarchean orogenic gold ore deposits: Stable isotopic and geochemical constraints with example from the Dharwar Craton, southern India. *Ore Geol. Rev.* **2019**, *107*, 754–779. https://doi.org/10.1016/j.oregeorev.2019.03.001

115. Champion, D.C.; Cassidy, K.F. *Granites of the Northern Murchison Province: Their Distribution, Age, Geochemistry, Petrogenesis, Relationship with Mineralisation, and Implications for Tectonic Environment*; AMIRA P482/MERIWA M281—Yilgarn Granitoids; AMIRA International (AMIRA P482 project consortium) and Minerals and Energy Research Institute of Western Australia (MERIWA): Perth, Western Australia, Australia, 2002; pp. 5.1–5.54.

116. Pitcairn, I.K.; Craw, D.; Teagle, D.A.H. The gold conveyor belt: Large-scale gold mobility in an active orogen. *Ore Geol. Rev.* **2014**, *62*, 129–142. https://doi.org/10.1016/j.oregeorev.2014.03.006

117. Connolly, J.A.D. The mechanics of metamorphic fluid expulsion. *Elements* **2010**, *6*, 165–172. https://doi.org/10.2113/gselements.6.3.165

118. Benning, L.G.; Seward, T.M. Hydrosulfide complexing of gold(I) in hydrothermal solutions from 150 to 500 °C and 500 to 1500 bars. *Geochim. Cosmochim. Acta* **1996**, *60*, 1849–1871. https://doi.org/10.1016/0016-7037(96)00061-0

119. Mikucki, E.J. Hydrothermal transport and depositional processes in Archean lode gold systems: A review. *Ore Geol. Rev.* **1998**, *13*, 307–321. https://doi.org/10.1016/S0169-1368(97)00025-5